AIMS Mathematics, 11(4): 11489–11519.
DOI: 10.3934/math.2026473
Received: 09 February 2026
Revised: 21 March 2026
Accepted: 13 April 2026
Published: 24 April 2026

https://www.aimspress.com/journal/Math

Research article

Fox H-function representations of temperature and displacement fields in unbounded domains with anomalous decelerating thermal conduction

Emad Awad[1] **and A. R. El-Dhaba**[2,*]

[1] Department of Mathematics, Faculty of Education, Alexandria University, Souter St. El-Shatby, Alexandria P.O. Box 21526, Egypt

[2] Department of Mathematics and Statistics, College of Science, King Faisal University, P.O. Box 400, Al-Ahsa 31982, Saudi Arabia

* **Correspondence:** Email: aemam@kfu.edu.sa.

Abstract: Recent advances in fractional calculus have highlighted the role of distributed-order operators in modeling anomalous diffusion processes, particularly through bi-fractional diffusion equations of the natural type. In this work, we introduce a distributed-order fractional integral formulation that leads to a generalized bi-fractional Fourier law involving two Riemann–Liouville fractional integrals. The proposed constitutive relation captures a class of anomalous heat conduction characterized by decelerating thermal transport, wherein the effective thermal conductivity is relatively large in the short-time regime and diminishes in the long-time regime. For a quasi-static thermoelastic problem in an unbounded domain, exact analytical solutions for the temperature and displacement fields are derived and expressed in terms of the Fox H-function. Within the quasi-static framework, it is rigorously shown that the appropriate zero initial condition must be imposed on the normal stress rather than on the volumetric strain. A damped cosinusoidal boundary condition at infinity is incorporated and is shown to affect the elastic response due to the infinite propagation speed of mechanical disturbances under the quasi-static assumption. The coupled thermo-mechanical analysis reveals that thermal and mechanical fields exhibit analogous transitional behavior: Decelerating thermal conduction induces a corresponding retardation in the deformation of the medium.

Keywords: asymptotic solutions ; Cauchy problem; Fox H-function; fractional calculus; quasistatic theory
Mathematics Subject Classification: 34A08, 35B40, 74B05, 80A20

1. Introduction

The thermal conduction properties in thermal transport systems must meet strict standards across various contemporary industrial sectors. A key aspect of this is that material's thermal conductivity should change with temperature instead of remaining constant [1, 2]. The thermal conductivity is frequently treated as a constant value fixed at room temperature for modeling scenarios wherein temperature-dependent properties are complex to address; see a very recent example [3]. The term "anomalous thermal conductivity" began to emerge in publications in the 1950s after Berman and Macdonald published their study [4]; see further examples in [5–7]. In the thermodynamic limit, the variation of thermal conductivity was studied in [8]. The authors also presented a possible illustration according to the framework of linear response theory through correlating the physical origin of the anomalous thermal conduction to the slow diffusion of energy from long-wavelength Fourier modes. Deviations from classical diffusion "Fourier" behavior arise from atypical substances, alloys with dissolved impurities, structures on the nanoscale, and the conduction of heat in fractals. The terminology "anomalous" was also used for the processes of heat conduction, wherein the carriers of thermal energy follow the power-law $\left\langle x^2(t)\right\rangle \propto t^{\alpha}$, $\alpha \in (0,2)$ [9]. Moreover, the thermal conductivity is said to be anomalous and deviates from the conventional definition when the energy carriers run into obstacles during the heat transfer process, taking on the form $\check{\kappa} = \kappa L^{\frac{2\alpha-2}{\alpha}}$; refer to [9]. As a result, thermal conductivity has two different anomalous expressions: The first is for the subdiffusion of energy carriers, $\left\langle x^2(t)\right\rangle \propto t^{\alpha}$, $\alpha \in (0,1)$, which yields "low thermal conductivity" $\check{\kappa} < \kappa$, provided that the characteristic length $L > 1$. The superdiffusion of energy carriers is the second instance, $\left\langle x^2(t)\right\rangle \propto t^{\alpha}$, $\alpha \in (1,2)$, which results in "high thermal conductivity" $\check{\kappa} > \kappa$, provided that the characteristic length $L > 1$. From an experimental viewpoint, these anomalies have been mentioned in various physical situations, see examples of ultrahigh thermal conductivity in millimeter-long nanotubes [10], experimental observations of high thermal conductivity in boron arsenide [11], ultralow thermal conductivity in TlCuSe [12], and ultrahigh thermal conductivity in graphene films [13]. Additionally, as observed in the third figure of the study by Li et al. [14], at temperatures close to room temperature ($T_0 = 300$ K), a silicon nanowire with a diameter of 22 nm exhibits an increase in thermal conductivity as the temperature rises. In contrast, a silicon nanowire with a diameter of 115 nm displays a notable decrease in thermal conductivity with increasing temperature, highlighting the significant influence of material size on thermal conductivity, and opening a debate around the kind of monotonic variation occurring in the thermal conduction, either with acceleration or deceleration.

In many pivotal fields, e.g., engineering, physics, and biology, fractional derivatives and integrals are primarily used in modeling a variety of natural phenomena through fractional kinetic equations, which, in turn, depict the exponent of mean-squared displacement for diffusive materials [15, 16]. An explicit demonstration of how crucial fractional calculus is for clarifying atypical behaviors can be seen in the fractional diffusion-wave equation proposed by Schneider and Wyss [17]. Among others, we refer to the generalized fractional diffusion equation of the natural type that uses the Caputo fractional derivative [18], and the modified type that uses the Riemann–Liouville fractional derivative [19] which shows different crossover behavior such as retardation and acceleration; see also their multidimensional counterparts in [20, 21]. Various contributions adding new perspectives to this type of bi-fractional equations are found in [22–24]. We refer also to a recent study on the fractional Jeffreys equation that

showed the transition from diffusion to a wave [25]. We further refer to some advanced numerical techniques on solving the fractional Jeffreys equation in [26, 27] and its fractional basis, the fractional two-temperature model [28]. In [29], Compte and Metzler discovered, while deriving the fractional telegrapher equation, that the anomalous diffusion coefficient is expressed as $D_\alpha = \sigma^2/\tau^\alpha$, while the conventional diffusion coefficient is $D = \sigma^2/\tau$. This finding led later to the alteration of a related equation for irregular thermal conduction [30]. Furthermore, the importance of fractional calculus is clearly shown in the possibility of finding damped oscillations in the presence of fractional kinetic equations [31].

Due to thermal deformations potentially leading elastic materials to reach the "yield point", anticipating this behavior during heat transfer processes is crucial. This necessitates a comprehensive theoretical analysis, especially when the mode of thermal conduction shifts. Biot [32] examined the Fourier heat transfer phenomenon, taking into account the thermal deformations caused by temperature changes, as well as the thermal energy resulting from these deformations. Emerging from the necessity for a finite speed of thermal wave propagation, a condition that the Biot model does not satisfy, a variety of thermoelasticity theories were formulated throughout the previous century [33]. Aiming to accommodate the nonlinear deformation in the presence of the Cattaneo-type evolution, a nonlinear theory of thermoelectricity was constructed in [34, 35]. On the basis of the Jeffreys-type heat conduction law, Tzou introduced a new version of the generalized thermoelasticity theory [36]. The first discussion of fractional theory thermoelasticity, which relies on the fractional diffusion–wave equation, was in [37]. Different versions of the fractional theory of thermoelasticity that were based on different forms of the time-fractional Cattaneo equation were examined between 2010 and 2011, by Sherief et al. [38], Youssef [39], Ezzat [40], and Povstenko [41]. Utilizing a fractional formulation of the dual-phase-lag heat conduction principle, a fractional dual-phase-lag thermoelasticity model was developed in [42], see also the most recent book on the fractional thermoelasticity [43]. Recently, a crossover model for heat conduction has been employed to emulate the transition from low thermal conductivity in the short-time frame to the high thermal conductivity for large time values, leading to the development of a crossover thermoelasticity theory as detailed in [44], Such a theory is useful to theoretically predict situations in which thermal conductivity varies temporally with acceleration. Exact solutions for stress and displacement have been obtained for an unbounded domain under the condition of quasistatic conserved momentum. The recent thermoelasticity theory with accelerated heat conduction process has been applied to cylindrical domains in [45], and to an unbounded electro-thermoelastic domain in [46].

In this study, a fractional theory of the quasi-static thermoelasticity is developed for an unbounded elastic domain, founded on a fractional generalized Fourier constitutive law that incorporates two Riemann-Liouville integrals of different fractional orders. The generalized Fourier law demonstrates a transitional behavior of the thermal conductivity over the time, where it initiates with a relatively high thermal conductivity during the very small time values, and eventually ends with a lower thermal conductivity for large time instants, i.e., a decelerating thermal conduction. Thus, the primary objective of this research is to investigate how this temporally decelerating crossover in thermal conductivity influences thermally-induced deformation. The structure of the paper is as follows: in Section 2, we introduce the fractional constitutive law which contains two Riemann-Liouville fractional integrals, and we show that this law has a temporal crossover characteristic. Moreover, we derive the governing equations of the quasistatic theory of thermoelasticity which uses this unfamiliar

law, and we show the method of solution which based on the usage of Laplace and Fourier transforms. Using the Fox H-function, we get explicit solutions for temperature and displacement in Section 3 that hold true for both short and long times. The temperature and displacement numerical approximations are the main topic of Section 4. Finally, we provide a summary of the paper's main findings in Section 5.

2. Mathematical formulation

In this section, we introduce a generalized Fourier constitutive law which exhibits a decelerating transition of thermal conduction. In addition, the quasi-static theory of fractional thermoelasticity that uses such a generalized is constructed.

2.1. Decelerating thermal conduction

The classical Fourier constitutive law describing the relation between the heat flux i-th component $q_i(x_i, t)$ with the temperature gradient $T_{,i}(x_i, t) = \partial T(x_i, t)/\partial x_i$ for an isotropic heat conductor reads:

$$q_i = -\kappa(T)\, T_{,i}, \tag{2.1}$$

where x_i is the i-th component of the coordinate system (x_1, x_2, x_3), t is the time, $T = T(x_i, t)$ is the absolute temperature, and $\kappa(T)$ is the thermal conductivity for the material. It is commonly recognized that thermal conductivity is a temperature-dependent property that varies as the material's temperature changes, refer to [1, 2]. For small temperature values, the thermal conductivity can be represented in the current series form [47, 48]

$$\kappa(\theta) = \kappa_0 + \kappa_1\theta + \mathrm{O}(\theta), \tag{2.2}$$

where $\theta = T - T_0$, T_0 is the room temperature, and κ_0 and κ_1 are real constants, and ($\kappa_0 > 0$) is the thermal conductivity at room temperature. However, in many modeling problems, thermal conductivity is treated as a fixed thermophysical property to avoid complication of numerical simulations [3], namely, $q_i = -\kappa_0 T_{,i}$. On the other hand, even in the small temperature values, Eq (2.2) shows that temperature variations have a significant impact on thermal conductivity, in the sense that it may cause a temporal increase or decrease according to the thermal settings of the experiment and the real constants κ_0 and κ_1. Therefore, treating thermal conductivity as a constant is not accurate.

Let us replace the conventional form of Fourier law (2.1) with the following generalized form, defined in terms of the distributed-order integral,

$$\int_0^1 \frac{P(\nu)}{\tau^{1-\nu}} \left\{ {}^{RL}_{0}I_t^{1-\nu} q_i(x,t) \right\} \mathrm{d}\nu = -\kappa_0 T_{,i}(x,t), \tag{2.3}$$

where τ is a time constant is inserted to keep the dimension in order, but it will play a key role in varying the thermal conduction of material later, and $P(\nu)$ is a weight function presumed to be normalized, i.e., $\int_0^1 P(\nu)\mathrm{d}\nu = 1$. Furthermore, ${}^{RL}_{0}I_t^{\nu}$ is the Riemann-Liouville fractional integral of order ν, $0 < \nu < 1$, defined for any generic function as [49]

$$ {}^{RL}_{0}I^{\nu}_{t} f(t) := \begin{cases} \dfrac{1}{\Gamma(\nu)} \displaystyle\int_0^t \frac{f(\tau)}{(t-\tau)^{1-\nu}} \mathrm{d}\tau, & \nu > 0, \\ f(t), & \nu = 0. \end{cases} \tag{2.4} $$

If we choose the weight function $P(\nu)$ on the following form

$$ P(\nu) = p_1 \delta(\nu - \alpha) + p_2 \delta(\nu - \beta), \tag{2.5} $$

where p_1 and p_2 are dimensionless positive real constants satisfying that $p_1 + p_2 = 1$ in accordance with the normalization condition of $P(\nu)$, and $0 < \alpha < \beta \leq 1$. Utilizing the assumption (2.5), the generalized Fourier law (2.3) reduces to the following form

$$ \frac{p_1}{\tau^{1-\alpha}} \left\{ {}^{RL}_{0}I^{1-\alpha}_{t} q_i(x,t) \right\} + \frac{p_2}{\tau^{1-\beta}} \left\{ {}^{RL}_{0}I^{1-\beta}_{t} q_i(x,t) \right\} = -\kappa_0 T_{,i}(x,t). \tag{2.6} $$

The bi-fractional generalized Fourier law (2.6) uses two Riemann-Liouville fractional integrals of distinct fractional orders. Bearing in mind that the constants p_1 and p_2 are dimensionless, the dimension of Eq (2.6) can be written as $[q_i] = [\kappa_0 T_{,i}]$ where the following approximation is utilized:

$$ \left\{ p_1 \left(\frac{t}{\tau}\right)^{1-\alpha} + p_2 \left(\frac{t}{\tau}\right)^{1-\beta} \right\} [q_i] = [\kappa_0 T_{,i}]. \tag{2.7} $$

In view of (2.7), for small values of time $t \ll \tau$, we have

$$ p_1 \left(\frac{t}{\tau}\right)^{1-\alpha} + p_2 \left(\frac{t}{\tau}\right)^{1-\beta} \cong p_2 \left(\frac{t}{\tau}\right)^{1-\beta}, \quad \alpha < \beta \leq 1, \tag{2.8} $$

provided $p_1 \leq p_2$. In this case the generalized Fourier constitutive law (2.6) reduces to

$$ \frac{p_2}{\tau^{1-\beta}} \left\{ {}^{RL}_{0}I^{1-\beta}_{t} q_i \right\} \cong -\kappa_0 T_{,i}, \quad t \ll \tau. \tag{2.9} $$

Applying the Riemann-Liouville fractional derivative ${}^{RL}_{0}\mathscr{D}^{1-\beta}_{t}$ of order $1-\beta$, $0 < \beta < 1$, defined for any generic function $f(t)$ as [49]

$$ {}^{RL}_{0}\mathscr{D}^{1-\beta}_{t} f(t) := \begin{cases} \dfrac{\mathrm{d}}{\mathrm{d}t} \left\{ {}^{RL}_{0}I^{\beta}_{t} f(t) \right\}, & 0 < \beta < 1, \\ \dfrac{\mathrm{d}f(t)}{\mathrm{d}t}, & \beta = 0, \\ f(t), & \beta = 1, \end{cases} \tag{2.10} $$

on both sides of Eq (2.9), we obtain

$$ q_i \cong -\kappa_\beta \, {}^{RL}_{0}\mathscr{D}^{1-\beta}_{t} T_{,i}, \quad t \ll \tau. \tag{2.11} $$

Following similar arguments, for large values of time $t \gg \tau$ the generalized Fourier constitutive law (2.6) reduces to

$$ q_i \cong -\kappa_\alpha \, {}^{RL}_{0}\mathscr{D}^{1-\alpha}_{t} T_{,i}, \quad t \gg \tau. \tag{2.12} $$

In the asymptotic behaviors (2.11) and (2.12), κ_α and κ_β are generalized thermal conductivities defined

$$\kappa_\alpha = \frac{\tau^{1-\alpha}}{p_1}\kappa_0, \quad \kappa_\beta = \frac{\tau^{1-\beta}}{p_2}\kappa_0. \tag{2.13}$$

In other words, the largest fractional order β dominates the short-time domain and the smallest fractional order α dominates the long-time domain. This fact was shown previously in [18] by calculating the mean squared displacement in fractional diffusion, see also the multidimensional case [20]. From a physical point of view, the asymptotic behaviors (2.11) and (2.12) indicate that the generalized Fourier law (2.6) corresponds to a classical Fourier law (2.1) with variable thermal conductivity, where there are two different thermal conductivities κ_α and κ_β dominating the long-time domain and the short-time domain respectively. Moreover, in view of the definitions of generalized thermal conductivities (2.13), we note that for the fixed value $\kappa_0 = 386$, which corresponds to the thermal conductivity of copper at room temperature $T_0 = 293.15$ K, the generalized thermal conductivities κ_α and κ_β are given as

$$\kappa_\alpha = 154.034 < 487.099 = \kappa_\beta, \tag{2.14}$$

where the other parameters are chosen as $\alpha = 0.3, \beta = 0.8$, $p_1 = p_2 = 0.5$, and $\tau = 0.1$. Therefore, the temporal transition for thermal conduction represented by asymptotic behaviors (2.11) and (2.12) states that generalized Fourier law (2.6) behaves in the short-time domain like a non-Fourier law with high thermal conductivity κ_β, and behaves in the long-time domain as a non-Fourier law with low thermal conductivity κ_α, i.e., "*a decelerating thermal conduction*".

Upon introducing the conservation of thermal energy, governed through the relation

$$-q_{i,i} = \varrho C_E \frac{\partial T}{\partial t}, \tag{2.15}$$

where ϱ is the density of the heat conductor and C_E is the specific heat capacity, and eliminating the heat flux between (2.6) and (2.15), we obtain the generalized heat conduction equation:

$$\varrho C_E \left(\frac{p_1}{\tau^{1-\alpha}} {}_0^C\mathscr{D}_t^\alpha + \frac{p_2}{\tau^{1-\beta}} {}_0^C\mathscr{D}_t^\beta \right) T = \kappa_0 T_{,ii}, \tag{2.16}$$

where ${}_0^C\mathscr{D}_t^\alpha$ the Caputo fractional derivative of order α, $0 < \alpha < 1$, defined for any generic function $f(t)$ as [49]

$${}_0^C\mathscr{D}_t^\alpha f(t) := \begin{cases} {}_0^{RL}I_t^{1-\alpha}\left\{\dfrac{\mathrm{d}f(t)}{\mathrm{d}t}\right\}, & 0 < \alpha < 1, \\ \dfrac{\mathrm{d}f(t)}{\mathrm{d}t}, & \alpha = 1, \\ f(t), & \alpha = 0. \end{cases} \tag{2.17}$$

In Eq (2.16), the fractional orders α and β $(0 < \alpha < \beta \leq 1)$ characterize the strength of memory effects in the thermal process. When $\alpha = \beta = 1$, the classical Fourier model is recovered, while lower values correspond to increasing nonlocality in time and decelerating heat propagation. The presence of two

fractional orders introduces multiple memory scales into the heat flux evolution. Unlike single-order models, this allows the thermal response to evolve through different temporal regimes, leading to a gradual slowdown (deceleration) of heat transfer. Thereby, the bi-fractional heat conduction equation (2.16) that uses a fixed value of the thermal conductivity, corresponds to a non-Fourier heat conduction law that simulates a decelerating temporal crossover of thermal conduction from high thermal conductivity in the short-time domain to a low thermal conductivity in the long-time domain. In the case of non-Fickian diffusion, Eq (2.16) was directly derived from the fractional diffusion equation of distributed order without referring to the role of flux, refer to [18, 20].

2.2. Governing equations

In this subsection, we will derive the governing equations of the theory of quasi-static thermoelasticity based on the generalized Fourier law (2.6). We focus our attention on the infinitesimal deformation of a homogeneous isotropic solid continuum defined in the sense of Hook's definition for perfect elastic materials. We suppose that deformation is induced by initial thermomechanical conditions. The momentum conservation equation, excluding volume and inertia forces, is a key field equation governing the movement of the thermoelastic medium. [33, 50]

$$\mu u_{i,jj} + (\lambda + \mu)\, u_{j,ji} - \gamma T_{,i} = 0. \tag{2.18}$$

The second governing equation is the thermal energy balance equation, excluding any internal heat sources, including strain-rate induced heat, and generalizing the simple form (2.15):

$$-\, q_{i.i} = \varrho C_E \frac{\partial T}{\partial t} + \gamma T_0\, \frac{\partial e}{\partial t}. \tag{2.19}$$

In the field equations (2.18) and (2.19), u_i is the i-th component of displacement, $e = \mathrm{tr}\left[e_{ij}\right] = e_{11} + e_{22} + e_{33}$ is the cubical dilation, and e_{ij} is the strain tensor defined as

$$e_{ij} = \frac{1}{2}\left(u_{i,j} + u_{j,i}\right). \tag{2.20}$$

Further, λ and μ are Lame moduli, $\gamma = (3\lambda + 2\mu)\,\alpha_T$, and α_T is the coefficient of linear thermal expansion. The constitutive equations for the above system of governing equations consists of the generalized Fourier law (2.6) and the stress-strain relation in the linearized form:

$$\sigma_{ij} = 2\mu e_{ij} + \lambda e \delta_{ij} - \gamma\,(T - T_0)\,\delta_{ij}, \tag{2.21}$$

where σ_{ij} is the stress tensor, and δ_{ij} is the Krönecker delta function.

If we eliminate the heat flux q_i between Eq (2.6) and (2.19), we obtain

$$\left(\frac{p_1}{\tau^{1-\alpha}}\,{}^{C}_{0}\mathscr{D}^{\alpha}_{t} + \frac{p_2}{\tau^{1-\beta}}\,{}^{C}_{0}\mathscr{D}^{\beta}_{t}\right)(\varrho C_E T + \gamma T_0 e) = \kappa_0 T_{,ii}. \tag{2.22}$$

Therefore, Eqs (2.18) and (2.22) are the governing equations for the quasi-static theory of thermoelasticity that uses a generalized Fourier constitutive law with decelerating thermal conduction. In Eq (2.18), it is worthy to note that the quasi-static assumption implies neglecting inertial terms in the equation of motion, which is justified when mechanical equilibration occurs much faster than thermal evolution. It should be noted that the decelerating thermal behavior arises from the heat conduction model and is independent of this assumption.

2.3. Unbounded thermomechanical continua

Here, we formulate the unbounded thermoelastic problem (or the thermoelastic initial-value problem) governed by (2.18) and (2.22) defined for a thermoelastic medium characterized by a decelerating thermal conductivity. We consider two sets of possible initial conditions; the first set is imposed on the temperature and stress [44]:

$$T(x,y,z,0) = T_0 + \vartheta_0 \delta(x), \quad \sigma_{xx}(x,y,z,0) = 0. \tag{2.23}$$

The second set of initial conditions is imposed on the temperature and the strain [46]:

$$T(x,y,z,0) = T_0 + \vartheta_0 \delta(x), \quad e(x,y,z,0) = 0, \tag{2.24}$$

where ϑ_0 is a positive real and $\delta(\cdot)$ is the Dirac delta function. In view of the initial conditions (2.23) and (2.24), the unbounded thermoelastic domain can be handled as a one-dimension application, in the sense that

$$T(x,y,z,t) = T(x,t), \quad \mathbf{u} = \langle u, 0, 0\rangle, \quad u(x,y,z,t) = u(x,t). \tag{2.25}$$

Therefore, the governing equations (2.18) and (2.22) can be written on the form

$$(\lambda + 2\mu)\frac{\partial^2 u}{\partial x^2} = \gamma \frac{\partial T}{\partial x}, \tag{2.26}$$

$$\left(\frac{p_1}{\tau^{1-\alpha}} {}_0^C\mathscr{D}_t^{\alpha} + \frac{p_2}{\tau^{1-\beta}} {}_0^C\mathscr{D}_t^{\beta}\right)\left(\varrho C_E T + \gamma T_0 \frac{\partial u}{\partial x}\right) = \kappa_0 \frac{\partial^2 T}{\partial x^2}. \tag{2.27}$$

Beside (2.26) and (2.27), the components of stress are given by

$$\sigma_{xx} = (\lambda + 2\mu)\frac{\partial u}{\partial x} - \gamma(T - T_0), \tag{2.28}$$

$$\sigma_{yy} = \sigma_{zz} = \lambda \frac{\partial u}{\partial x} - \gamma(T - T_0). \tag{2.29}$$

In the first set of initial conditions (2.23), the second condition reporting the initially unstressed medium state, $\sigma_{xx}(x,0) = 0$, has a physical interpretation in the case of one-dimension quasistatic problems. Indeed, from the equation of motion of the one-dimensional quasistatic settings we have that $\partial \sigma_{xx}(x,t)/\partial x = 0$, namely, $\sigma_{xx}(x,t) = \sigma_0(t)$. The function $\sigma_0(t)$ can be set to zero in unbounded domains since the stress is symmetric and may disappear as $x \to \pm\infty$. For this reason, we may accept the starting condition $\sigma_{xx}(x,0) = 0$, and the normal stress component $\sigma_{xx}(x,t)$ disappears everywhere, namely,

$$\sigma_{xx}(x,t) = 0. \tag{2.30}$$

utilizing equality (2.30), the hydrostatic stress for the first set of initial conditions is defined through

$$\sigma_H = \frac{\sigma_{xx} + \sigma_{yy} + \sigma_{zz}}{3} = \frac{2}{3}\left[\lambda \frac{\partial u}{\partial x} - \gamma(T - T_0)\right], \tag{2.31}$$

In the second set of initial conditions (2.24), the second condition reads $\partial u(x,0)/\partial x = 0$, which implies upon substituting into the constitutive equation (2.28) that

$$\sigma_{xx}(x,0) = -\gamma\vartheta_0\delta(x). \tag{2.32}$$

It is clear that the initial condition (2.32) resulting from the second set (2.24) contradicts the quasistatic assumption in which $\sigma_{xx}(x,t) = \sigma_0(t)$. Therefore, the second set of initial conditions cannot be applied in the current problem and will be excluded from the next analysis. Indeed, imposing the initial condition $e(x,0) = 0$ is not compatible with the quasi-static assumption. In the absence of inertial effects, the mechanical response is governed by an instantaneous equilibrium between stress and deformation. Therefore, any non-zero thermal field would immediately generate strain through thermoelastic coupling. Enforcing zero strain at the initial instant would contradict this equilibrium and imply an unphysical instantaneous constraint. Accordingly, the condition $\sigma_x x(x,0) = 0$ is adopted as a physically consistent initial condition. Using the stress component (2.28) and settings (2.25), the first set of initial conditions (2.23) can be rewritten in the following form

$$T(x,0) - T_0 = \vartheta_0\delta(x), \quad \frac{\partial u(x,0)}{\partial x} = \frac{\gamma\vartheta_0}{\lambda+2\mu}\delta(x), \tag{2.33}$$

where the second condition cannot be set to zero to prevent the first set (2.23) from being reduced to the second disregarded set (2.24). Furthermore, by integrating the second initial condition of (2.33) over the interval $(-\infty, x]$, and set $u(-\infty,0) = u_{-\infty}$, we obtain the alternative initial condition that should be imposed on the displacement instead of the cubical dilation:

$$u(x,0) = u_{-\infty} + \frac{\chi_0\vartheta_0}{\lambda+2\mu}\begin{cases} 1, & x > 0, \\ \dfrac{1}{2}, & x = 0, \\ 0, & x < 0. \end{cases} \tag{2.34}$$

Let us define the dimensionless transformations as follows:

$$\begin{gathered} x \to \frac{x}{c_1\eta}, \quad u \to \frac{u}{c_1\eta}, \quad u_{-\infty} \to \frac{U_{-\infty}}{c_1\eta}, \quad t \to \frac{t}{c_1^2\eta}, \quad \tau \to \frac{\tau}{c_1^2\eta}, \\ \left(\sigma_{ij},\ \sigma_H\right) \to (\lambda+2\mu)\left(\sigma_{ij},\ \sigma_H\right), \quad T \to \frac{\lambda+2\mu}{\gamma}\theta + T_0, \end{gathered} \tag{2.35}$$

where $c_1^2 = \frac{\lambda+2\mu}{\rho}$ and $\eta = \frac{\rho C_E}{\kappa}$. Then, applying the dimensionless transformation (2.35) on the governing equations (2.26) and (2.27), the stress components (2.28)–(2.30), and the initial conditions (2.33) and (2.34), we obtain

$$\frac{\partial u}{\partial x} = \theta, \tag{2.36}$$

$$\left(\frac{p_1}{\tau^{1-\alpha}}{}_0^C\mathscr{D}_t^\alpha + \frac{p_2}{\tau^{1-\beta}}{}_0^C\mathscr{D}_t^\beta\right)\left(\theta + \varepsilon_0\frac{\partial u}{\partial x}\right) = \frac{\partial^2\theta}{\partial x^2}, \tag{2.37}$$

$$\sigma_H = \frac{2}{3}(\delta_0 - 1)\theta, \tag{2.38}$$

$$\theta(x,0)=\Theta_0\delta(x),\quad \frac{\partial u(x,0)}{\partial x}=\Theta_0\delta(x),\quad u(x,0)=U_{-\infty}+\Theta_0\begin{cases}1, & x>0,\\ \frac{1}{2}, & x=0,\\ 0, & x<0.\end{cases} \tag{2.39}$$

where Eqs (2.26), (2.28) and (2.30) have been utilized in deriving equation (2.36), and the problem constants ε_0, δ_0, and Θ_0 are given by

$$\varepsilon_0=\frac{\gamma^2T_0}{\rho C_E(\lambda+2\mu)},\quad \delta_0=\frac{\lambda}{\lambda+2\mu},\quad \Theta_0=\frac{\gamma\vartheta_0c_1\eta}{\lambda+2\mu}, \tag{2.40}$$

and the constant ε_0 is called the thermomechanical coupling parameter which incorporates the mechanical effects in production of the thermal energy. In the case $\varepsilon_0=0$, such coupling is neglected and Eq (2.37) reduces to the bi-fractional diffusion equation of the natural type [20, 51].

2.4. Method of solution

In this subsection, we present the method of solution which helps in extracting exact solutions in the short-time and the long-time domains in the next section. Additionally, we investigate whether the thermomechanical coupling still maintains the temperature's non-negativity. First, we apply Laplace transform on Eqs (2.36) and (2.37) and use of the initial conditions (2.39), we obtain the temperature in the Laplace space as

$$\frac{\mathrm{d}^2\widetilde{\theta}(x,s)}{\mathrm{d}x^2}=(1+\varepsilon_0)\left\{\left(\frac{p_1s^\alpha}{\tau^{1-\alpha}}+\frac{p_2s^\beta}{\tau^{1-\beta}}\right)\widetilde{\theta}(x,s)-\left(\frac{p_1s^{\alpha-1}}{\tau^{1-\alpha}}+\frac{p_2s^{\beta-1}}{\tau^{1-\beta}}\right)\Theta_0\delta(x)\right\}, \tag{2.41}$$

where the tildes refer to the Laplace transform defined for any generic function as $\tilde{f}(x,s)=\mathscr{L}\{f(x,t);t\}(x,s)=\int_0^\infty f(x,t)\exp(-st)dt$, and $s\in\mathbb{C}$ is the Laplace parameter. Next, we apply the Fourier transform on (2.41), we obtain the temperature in the Laplace-Fourier space

$$\widehat{\widetilde{\theta}}(\omega,s)=\frac{\Theta_0(1+\varepsilon_0)\left(\frac{p_1s^{\alpha-1}}{\tau^{1-\alpha}}+\frac{p_2s^{\beta-1}}{\tau^{1-\beta}}\right)}{(1+\varepsilon_0)\left(\frac{p_1s^\alpha}{\tau^{1-\alpha}}+\frac{p_2s^\beta}{\tau^{1-\beta}}\right)+\omega^2}, \tag{2.42}$$

where the hats refer to the Fourier transform $\hat{f}(\omega,t)=\mathscr{F}\{f(x,t);x\}(\omega,t)=\int_{-\infty}^{\infty}f(x,t)\,e^{-\iota\omega x}\mathrm{d}x$, and $\omega\in\mathbb{R}$ is Fourier parameter.

A significant inquiry regarding the temperature arising from thermomechanical coupling ($\varepsilon_0\neq0$), (2.42), pertains to its nonnegativity and the preservation of thermal energy [52,53]. Firstly, by inverting the Fourier transform in (2.42), we derive

$$\widetilde{\theta}(x,s)=\frac{\Theta_0\sqrt{(1+\varepsilon_0)\psi(s)}}{2s}\exp\left(-\sqrt{(1+\varepsilon_0)\psi(s)}\,|x|\right),\quad \psi(s)=\frac{p_1s^\alpha}{\tau^{1-\alpha}}+\frac{p_2s^\beta}{\tau^{1-\beta}}. \tag{2.43}$$

Given (2.43), we observe that, if we set $\varepsilon_0=0$, the solution in the Laplace space corresponds to its counterpart in the case of anomalous diffusion, refer to [Eq (42) in [20]]. Additionally, when the Laplace parameter is established along the positive real axis, the impact of the factor $\sqrt{1+\varepsilon_0}$ within and outside the exponential function does not change the fundamental characteristic of temperature as a completely monotone function, which is expressed as the product of two completely monotone

functions: $\sqrt{\psi(s)}/s$ and $\exp\left(-\sqrt{(1+\varepsilon_0)\psi(s)}\,|x|\right)$. Thus, in the context of quasi-static fractional theory of thermoelasticity, employing the generalized Fourier constitutive law (2.6), which illustrates a unique behavior of diminishing thermal conduction, the nonnegativity of temperature $\theta(x,t)$ on $\mathbb{R}\times\mathbb{R}_+\cup\{0\}$ is preserved. It is important to highlight that the nonnegativity should be reconsidered in the dynamic theory that takes the inertia force $\varrho\partial^2 u/\partial t^2$ into account. Secondly, when we integrate both sides of (2.32) on $\mathbb{R}$, and next invert the Laplace transform, we obtain

$$\int_{-\infty}^{\infty}\theta(x,t)\mathrm{d}x=\Theta_0\mathscr{H}(t), \tag{2.44}$$

where $\mathscr{H}(t)$ is the Heaviside unit step function. More precisely, when we examine the total thermal energy provided by (2.44) in relation to the initial condition (2.39), which specifies a constant initial value Θ_0 for the temperature at the interfacial surface $x=0$, we can conclude that thermal energy is not changed during the heat transfer mechanism within the framework of the quasistatic theory of thermoelasticity, which employs the generalized Fourier constitutive law (2.6) describing the decelerating thermal conduction property.

3. Short- and long-time exact solutions

In this section, we develop exact solutions for dimensionless forms of temperature $\theta(x,t)$, hydrostatic stress $\sigma_H(x,t)$, and displacement $u(x,t)$ in the short- and long-time domains. The exact solution was firstly obtained for the bi-fractional diffusion equation of the natural form in [54] in terms of the Fox H-function. In [51], it was indicated that the solution derived in [54] is asymptotic rather than exact, demonstrating that it is effective for small- and intermediate-time values, but it may become divergent for larger time values. We also mention comparable handling methods that were implemented in [20]. Strictly speaking, a plausible recommendation was made to improve the time interval for which the solution remains valid, suggesting that the constants p_1 and p_2 be chosen with $p_1<p_2$. However, this proposal lacks a solid physical basis. Here, we present two formulations for the temperature: one applicable to small time values, and the other suitable for intermediate and large time values. To begin, we will restate Eq (2.42) in two equivalent forms:

$$\begin{aligned}
\widetilde{\widetilde{\theta}}(\omega,s)&=\frac{\Theta_0(1+\varepsilon_0)\left(\frac{p_1 s^{\alpha-1}}{\tau^{1-\alpha}}+\frac{p_2 s^{\beta-1}}{\tau^{1-\beta}}\right)}{\frac{p_2(1+\varepsilon_0)}{\tau^{1-\beta}}s^{\beta}+\omega^2}\left[1+\varphi_1(\omega,s)\right]^{-1},\\
\widetilde{\widetilde{\theta}}(\omega,s)&=\frac{\Theta_0(1+\varepsilon_0)\left(\frac{p_1 s^{\alpha-1}}{\tau^{1-\alpha}}+\frac{p_2 s^{\beta-1}}{\tau^{1-\beta}}\right)}{\frac{p_1(1+\varepsilon_0)}{\tau^{1-\alpha}}s^{\alpha}+\omega^2}\left[1+\varphi_2(\omega,s)\right]^{-1},
\end{aligned} \tag{3.1}$$

where the auxiliary functions $\varphi_1(\omega,s)$ and $\varphi_2(\omega,s)$ are given by

$$\varphi_1(\omega,s)=\frac{\frac{p_1(1+\varepsilon_0)}{\tau^{1-\alpha}}s^{\alpha}}{\frac{p_2(1+\varepsilon_0)}{\tau^{1-\beta}}s^{\beta}+\omega^2},\quad \varphi_2(\omega,s)=\frac{\frac{p_2(1+\varepsilon_0)}{\tau^{1-\beta}}s^{\beta}}{\frac{p_1(1+\varepsilon_0)}{\tau^{1-\alpha}}s^{\alpha}+\omega^2}. \tag{3.2}$$

To invert the Laplace and Fourier transform in (3.1), we should expand firstly $\left[1+\varphi_1(\omega,s)\right]^{-1}$ and $\left[1+\varphi_2(\omega,s)\right]^{-1}$, in other words, we should apply the expansion $(1+\varsigma)^{-1}=\sum_{n=0}^{\infty}(-\varsigma)^n$ which requires

that $|\varsigma| < 1$. A question has now arisen: Do the auxiliary functions $\varphi_1(\omega, s)$ and $\varphi_2(\omega, s)$ satisfy this condition? To answer this question, we illustrate the auxiliary functions $\varphi_1(\omega, s)$ and $\varphi_2(\omega, s)$ graphically by selecting $p_1 = p_2 = 0.5$, $\tau = 0.1$, $\alpha = 0.3$, $\beta = 0.8$, and $\varepsilon_0 = 0.0168$, along with various values of ω in Figure 1.

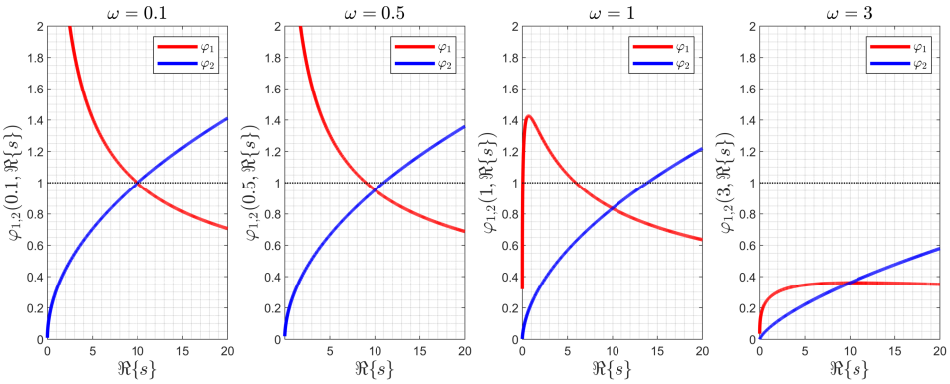

Figure 1. The auxiliary functions $\varphi_1(\omega, s)$ and $\varphi_2(\omega, s)$ for the generic selections $p_1 = p_2 = 0.5$, $\tau = 0.1$, $\alpha = 0.3$, $\beta = 0.8$, and $\varepsilon_0 = 0.0168$, and different values of the Fourier parameter ω: (a) $\omega = 0.1$, (b) $\omega = 0.5$, (c) $\omega = 1$, (d) $\omega = 3$.

It is widely acknowledged that the small values of the Fourier parameter ω correspond to the large values of the spatial variable x, and vice versa. Moreover, the small values of the Laplace parameter s correspond to the large values of the time variable t, and the converse is correct. In view of Figure 1, we note that for sufficiently large values of ω, both auxiliary functions are less than 1, which indicates that the solutions resulting from Eq (3.1) are unlikely to diverge for small and intermediate values of the spatial variable x, but the divergence for large values of x. In addition, for relatively large values of x, see Figure 1 a–c, the auxiliary functions satisfy the following conditions:

$$\varphi_1(\omega, s) < 1 \quad \text{for} \quad \Re\{s\} > 10, \qquad \varphi_2(\omega, s) < 1 \quad \text{for} \quad \Re\{s\} < 10. \tag{3.3}$$

The number $\Re\{s\} = 10$ depends on the choice of the time constant τ, refer to [44], wherein the choice of $\tau = 1$ yields the turning point $\Re\{s\} \lesseqgtr 1$. Therefore, utilizing the inequalities of (3.3), the Equations of (3.1) can be written as

$$\begin{aligned}\widehat{\widetilde{\theta}}(\omega, s) = \Theta_0 \sum_{n=0}^{\infty} \left(-\frac{p_1}{p_2}\tau^{\alpha-\beta}\right)^n \frac{s^{\beta-1+\alpha n}}{\left(s^\beta + \frac{\tau^{1-\beta}}{p_2(1+\varepsilon_0)}\omega^2\right)^{n+1}} \\ + \Theta_0 \frac{p_1}{p_2}\tau^{\alpha-\beta} \sum_{n=0}^{\infty} \left(-\frac{p_1}{p_2}\tau^{\alpha-\beta}\right)^n \frac{s^{\alpha-1+\alpha n}}{\left(s^\beta + \frac{\tau^{1-\beta}}{p_2(1+\varepsilon_0)}\omega^2\right)^{n+1}}, \quad \Re\{s\} \to \infty,\end{aligned} \tag{3.4}$$

$$\widehat{\widetilde{\theta}}(\omega, s) = \Theta_0 \sum_{n=0}^{\infty} \left(-\frac{p_2}{p_1}\tau^{\beta-\alpha}\right)^n \frac{s^{\alpha-1+\beta n}}{\left(s^\alpha + \frac{\tau^{1-\alpha}}{p_1(1+\varepsilon_0)}\omega^2\right)^{n+1}}$$

$$+\Theta_0 \frac{p_2}{p_1}\tau^{\beta-\alpha}\sum_{n=0}^{\infty}\left(-\frac{p_2}{p_1}\tau^{\beta-\alpha}\right)^n \frac{s^{\beta-1+\beta n}}{\left(s^\alpha+\frac{\tau^{1-\alpha}}{p_1(1+\varepsilon_0)}\omega^2\right)^{n+1}}, \quad \Re\{s\}\to 0. \tag{3.5}$$

Considering the two asymptotic solutions in the Laplace-Fourier domain for $\Re\{s\}\to\infty$, (3.4), and for $\Re\{s\}\to 0$, (3.5), we observe that they can be commuted through the transformations:

$$\alpha \longleftrightarrow \beta, \quad p_1 \longleftrightarrow p_2. \tag{3.6}$$

Now, by inverting the Laplace transform of Eqs (3.4) using the useful relation (A.2), we obtain the temperature values for short-time domain within the Fourier domain:

$$\begin{aligned}\widehat{\theta}(\omega,t) = \Theta_0 \sum_{n=0}^{\infty}\left[-\frac{p_1}{p_2}\left(\frac{t}{\tau}\right)^{\beta-\alpha}\right]^n E^{n+1}_{\beta,(\beta-\alpha)n+1}\left(-\frac{\tau^{1-\beta}t^\beta}{p_2(1+\varepsilon_0)}\omega^2\right)\\ +\Theta_0\frac{p_1}{p_2}\left(\frac{t}{\tau}\right)^{\beta-\alpha}\sum_{n=0}^{\infty}\left[-\frac{p_1}{p_2}\left(\frac{t}{\tau}\right)^{\beta-\alpha}\right]^n E^{n+1}_{\beta,(\beta-\alpha)(n+1)+1}\left(-\frac{\tau^{1-\beta}t^\beta}{p_2(1+\varepsilon_0)}\omega^2\right), \quad t<\tau.\end{aligned} \tag{3.7}$$

Using the relations (A.3), (A.7) and (A.8), we obtain the exact solution for the temperature performs effectively for small values of time as

$$\theta(x,t) = \Theta_0\sqrt{\frac{p_2(1+\varepsilon_0)}{4\pi\tau^{1-\beta}t^\beta}}\left\{\theta_{s1}(x,t)+\frac{p_1}{p_2}\left(\frac{t}{\tau}\right)^{\beta-\alpha}\theta_{s2}(x,t)\right\}, \quad t<\tau, \tag{3.8}$$

where $\theta_{s1}(x,t)$ and $\theta_{s2}(x,t)$ are given as

$$\begin{aligned}\theta_{s1}(x,t) &= \sum_{n=0}^{\infty}\frac{(-1)^n}{n!}\left[\frac{p_1}{p_2}\left(\frac{t}{\tau}\right)^{\beta-\alpha}\right]^n H^{2,0}_{1,2}\left[\frac{p_2(1+\varepsilon_0)x^2}{4\tau^{1-\beta}t^\beta}\,\middle|\,\begin{matrix}\left(1+(\beta-\alpha)n-\frac{\beta}{2},\beta\right)\\(0,1),\left(\frac{1}{2}+n,1\right)\end{matrix}\right],\\ \theta_{s2}(x,t) &= \sum_{n=0}^{\infty}\frac{(-1)^n}{n!}\left[\frac{p_1}{p_2}\left(\frac{t}{\tau}\right)^{\beta-\alpha}\right]^n H^{2,0}_{1,2}\left[\frac{p_2(1+\varepsilon_0)x^2}{4\tau^{1-\beta}t^\beta}\,\middle|\,\begin{matrix}\left(1+(\beta-\alpha)(n+1)-\frac{\beta}{2},\beta\right)\\(0,1),\left(\frac{1}{2}+n,1\right)\end{matrix}\right].\end{aligned} \tag{3.9}$$

According to the asymptotic behaviors of the generalized Fourier law (2.6), refer to (2.11) and (2.12), in the very small values of time the energy balance equation (2.37) reduces to

$$\frac{p_2}{\tau^{1-\beta}}\,{}^{C}_{0}\mathscr{D}^{\beta}_{t}\left(\theta+\varepsilon_0\frac{\partial u}{\partial x}\right) = \frac{\partial^2\theta}{\partial x^2}, \tag{3.10}$$

which leads to the temperature solution on the form

$$\theta_\beta(x,t) = \Theta_0\sqrt{\frac{p_2(1+\varepsilon_0)}{4\pi\tau^{1-\beta}t^\beta}}H^{2,0}_{1,2}\left[\frac{p_2(1+\varepsilon_0)x^2}{4\tau^{1-\beta}t^\beta}\,\middle|\,\begin{matrix}\left(1-\frac{\beta}{2},\beta\right)\\(0,1),\left(\frac{1}{2},1\right)\end{matrix}\right], \quad t\to 0. \tag{3.11}$$

The existence of the thermomechanical coupling $\varepsilon_0 \neq 0$, which results from the influence of mechanical variables on temperature fluctuations, is the crucial element of the closed-form solutions (3.8) and (3.9) for short time domain and (3.11) for very small values of time. In the absence of this effect, i.e., $\varepsilon_0 = 0$, Eq (3.8) reduces to the solution of the bi-fractional diffusion equation of the natural

type [20, 51, 54]. However, the solution (3.8) and (3.9) when $\varepsilon_0 = 0$ was claimed as exact solution [54]. Here we subdivide the solutions to short-time domain solution and long-time-domain solution as we shall validate this claim in the next section.

The displacement for the short-time domain can be derived by solving Eq (2.36) together with the solution (3.8) and (3.9). Firstly, by integrating both sides of (2.36) over the interval $(-\infty, x]$, we obtain

$$u(x,t) = U_{-\infty}(t) + \int_{-\infty}^{x} \theta(\xi,t)\mathrm{d}\xi, \tag{3.12}$$

where $U_{-\infty}(t) = u(-\infty,t)$ is the time-dependent boundary condition at $x \to -\infty$. We may choose the following generic function

$$U_{-\infty}(t) = U_{-\infty}\exp(-at)\cos(bt), \tag{3.13}$$

noting that $U_{-\infty}(0) = u(-\infty,0) = U_{-\infty}$ agrees well with the initial condition (2.39). Secondly, the integral in (3.12) can be subdivided into $\int_{-\infty}^{x}\theta(\xi,t)\mathrm{d}\xi = \int_{-\infty}^{0}\theta(\xi,t)\mathrm{d}\xi + \int_{0}^{x}\theta(\xi,t)\mathrm{d}\xi$, where the first integral can be evaluated from (2.44) as

$$u(x,t) = U_{-\infty}\exp(-at)\cos(bt) + \frac{\Theta_0}{2}\mathscr{H}(t) + \int_{0}^{x}\theta(\xi,t)\mathrm{d}\xi. \tag{3.14}$$

The integral of (3.14) can be calculated by using the Euler transform of the Fox H-function (A.9) when one incorporates the short-time domain solution (3.8) and (3.9). We finally obtain the short-time domain exact form for the displacement as

$$\begin{aligned} u(x,t) = U_{-\infty}\exp(-at)\cos(bt) &+ \frac{\Theta_0}{2}\mathscr{H}(t) \\ &+\Theta_0\sqrt{\frac{p_2(1+\varepsilon_0)}{4\pi\tau^{1-\beta}t^{\beta}}}\operatorname{sign}(x)|x|\left\{u_{s1}(x,t) + \frac{p_1}{p_2}\left(\frac{t}{\tau}\right)^{\beta-\alpha}u_{s2}(x,t)\right\}, \quad t<\tau, \end{aligned} \tag{3.15}$$

where $u_{s1}(x,t)$ and $u_{s2}(x,t)$ are given by

$$\begin{aligned} u_{s1}(x,t) &= \sum_{n=0}^{\infty}\frac{(-1)^n}{n!}\left[\frac{p_1}{p_2}\left(\frac{t}{\tau}\right)^{\beta-\alpha}\right]^n H_{2,3}^{2,1}\left[\frac{p_2(1+\varepsilon_0)x^2}{4\tau^{1-\beta}t^{\beta}}\,\middle|\,\begin{matrix}(0,2);\left(1+(\beta-\alpha)n-\frac{\beta}{2},\beta\right)\\ (0,1),\left(\frac{1}{2}+n,1\right);(-1,2)\end{matrix}\right], \\ u_{s2}(x,t) &= \sum_{n=0}^{\infty}\frac{(-1)^n}{n!}\left[\frac{p_1}{p_2}\left(\frac{t}{\tau}\right)^{\beta-\alpha}\right]^n H_{2,3}^{2,1}\left[\frac{p_2(1+\varepsilon_0)x^2}{4\tau^{1-\beta}t^{\beta}}\,\middle|\,\begin{matrix}(0,2);\left(1+(\beta-\alpha)(n+1)-\frac{\beta}{2},\beta\right)\\ (0,1),\left(\frac{1}{2}+n,1\right);(-1,2)\end{matrix}\right]. \end{aligned} \tag{3.16}$$

Also, we can derive the displacement solution which is valid for the very small values of time $t \to 0$ by inserting the temperature solution $\theta_\beta(x,t)$ given by (3.11) into (3.14) and applying the Euler transform relation (A.9), we obtain

$$\begin{aligned} u_\beta(x,t) = U_{-\infty}\exp(-at)\cos(bt) &+ \frac{\Theta_0}{2}\mathscr{H}(t) \\ &+\Theta_0\sqrt{\frac{p_2(1+\varepsilon_0)}{4\pi\tau^{1-\beta}t^{\beta}}}H_{2,3}^{2,1}\left[\frac{p_2(1+\varepsilon_0)x^2}{4\tau^{1-\beta}t^{\beta}}\,\middle|\,\begin{matrix}(0,2);\left(1-\frac{\beta}{2},\beta\right)\\ (0,1),\left(\frac{1}{2},1\right);(-1,2)\end{matrix}\right], \quad t\to 0 \end{aligned} \tag{3.17}$$

It is worth noting that $\theta_\beta(x,t)$ can be extracted from (3.8), and $u_\beta(x,t)$ can be obtained from (3.15) by setting $p_1 = 0$. The following limits hold true

$$\lim_{t\to 0}\theta(x,t) = \theta_\beta(x,t), \quad \lim_{t\to 0}u(x,t) = u_\beta(x,t). \tag{3.18}$$

From a mathematical point of view, deriving the intermediate- and long-time domain temperature solution from (3.5) by following similar steps to the above is problematic since we encounter the inverse Laplace of the term

$$\mathscr{L}^{-1}\left\{\frac{s^{\alpha(n+1)-((\alpha-\beta)n+1)}}{\left(s^\alpha + \frac{\tau^{1-\alpha}}{p_1(1+\varepsilon_0)}\omega^2\right)^{n+1}}\right\},$$

where $((\alpha-\beta)n+1) < 0$ for $n \geq 1$, which contradicts the requirement of Eq (A.2). This controversial step can be skipped by applying the transformations (3.6) in an intuitive way, we finally get the temperature solution for the intermediate and large values of time as

$$\theta(x,t) = \Theta_0\sqrt{\frac{p_1(1+\varepsilon_0)}{4\pi\tau^{1-\alpha}t^\alpha}}\left\{\theta_{l1}(x,t) + \frac{p_2}{p_1}\left(\frac{t}{\tau}\right)^{\alpha-\beta}\theta_{l2}(x,t)\right\}, \quad t > \tau, \tag{3.19}$$

where $\theta_{l1}(x,t)$ and $\theta_{l2}(x,t)$ are given as

$$\begin{aligned}
\theta_{l1}(x,t) &= \sum_{n=0}^{\infty}\frac{(-1)^n}{n!}\left[\frac{p_2}{p_1}\left(\frac{t}{\tau}\right)^{\alpha-\beta}\right]^n H_{1,2}^{2,0}\left[\frac{p_1(1+\varepsilon_0)x^2}{4\tau^{1-\alpha}t^\alpha}\,\middle|\,\begin{matrix}\left(1+(\alpha-\beta)n-\frac{\alpha}{2},\alpha\right)\\ (0,1),\left(\frac{1}{2}+n,1\right)\end{matrix}\right],\\
\theta_{l2}(x,t) &= \sum_{n=0}^{\infty}\frac{(-1)^n}{n!}\left[\frac{p_2}{p_1}\left(\frac{t}{\tau}\right)^{\alpha-\beta}\right]^n H_{1,2}^{2,0}\left[\frac{p_1(1+\varepsilon_0)x^2}{4\tau^{1-\alpha}t^\alpha}\,\middle|\,\begin{matrix}\left(1+(\alpha-\beta)(n+1)-\frac{\alpha}{2},\alpha\right)\\ (0,1),\left(\frac{1}{2}+n,1\right)\end{matrix}\right].
\end{aligned} \tag{3.20}$$

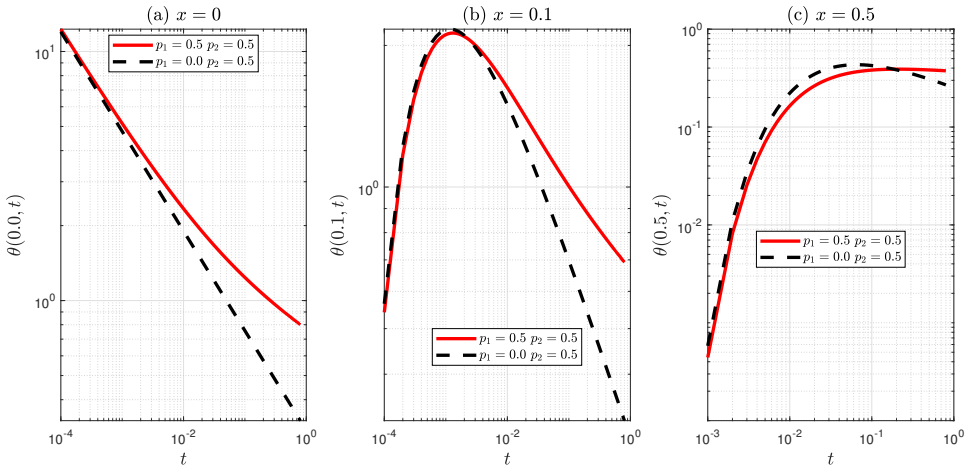

Figure 2. The short-time temperature solution (3.8)-(3.9) at different positions (red curve) and the temperature solution (3.11) of fractional thermoelasticity theory that utilizes the generalized thermal energy balance equation (3.10) (black dashed curve) on the log-log scale. (a) $x = 0$; (b) $x = 0.1$; (c) $x = 0.5$.

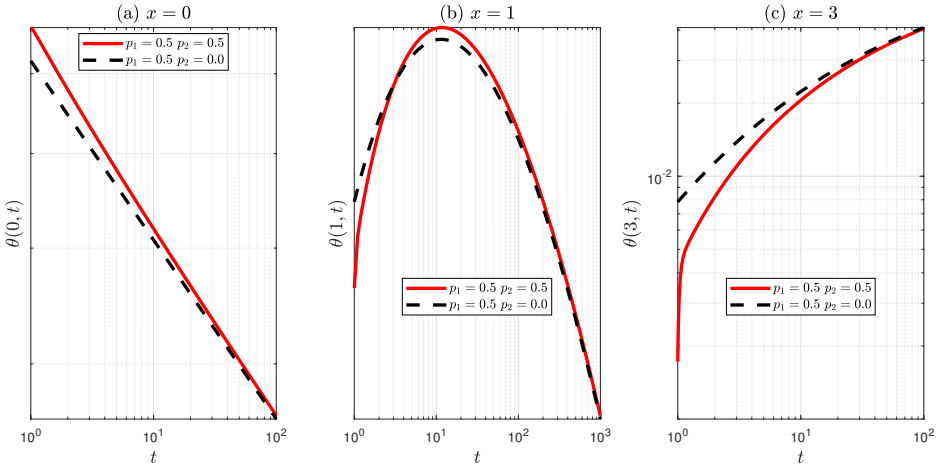

Figure 3. The long-time temperature solution (3.19)-(3.20) at different positions (red curve) and the temperature solution (3.21) of fractional thermoelasticity theory (black dashed curve) on the log-log scale. (a) $x = 0$; (b) $x = 1$; (c) $x = 3$.

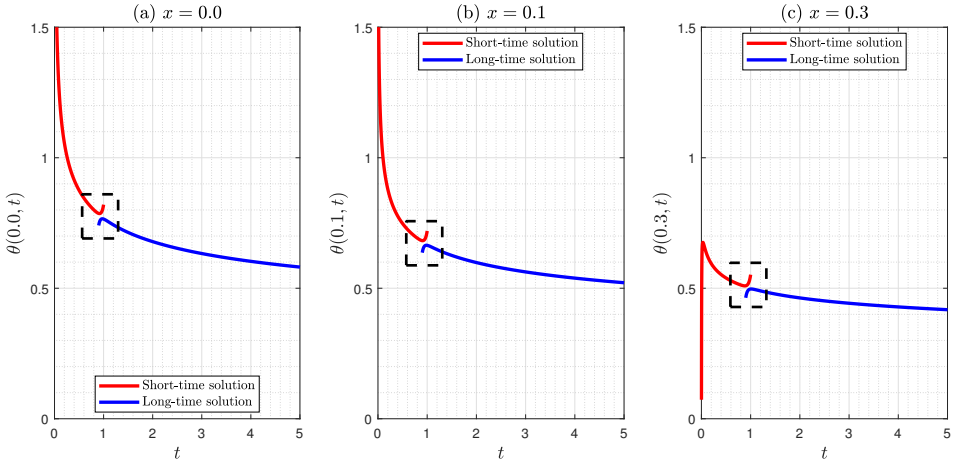

Figure 4. Temporal evolution of the short-time and the long-time temperature solutions (3.8)-(3.9) and (3.19)-(3.20), respectively, at different positions: (a) $x = 0$; (b) $x = 0.1$; (c) $x = 0.5$.

In addition, the temperature solution for the very large values of time $t \to \infty$ is given by applying the transformations (3.6) on (3.11), we get

$$\theta_\alpha(x,t) = \Theta_0 \sqrt{\frac{p_1(1+\varepsilon_0)}{4\pi\tau^{1-\alpha}t^\alpha}} H^{2,0}_{1,2}\left[\frac{p_1(1+\varepsilon_0)x^2}{4\tau^{1-\alpha}t^\alpha}\,\middle|\,\begin{matrix}\left(1-\frac{\alpha}{2},\alpha\right)\\(0,1),\left(\frac{1}{2},1\right)\end{matrix}\right], \quad t \to \infty. \tag{3.21}$$

Finally, the displacement for the intermediate- and long-time domains is given as

$$\begin{aligned} u(x,t) = U_{-\infty}&\exp(-at)\cos(bt) + \frac{\Theta_0}{2}\mathscr{H}(t) \\ &+\Theta_0\sqrt{\frac{p_1(1+\varepsilon_0)}{4\pi\tau^{1-\alpha}t^\alpha}}\operatorname{sign}(x)|x|\left\{u_{l1}(x,t) + \frac{p_2}{p_1}\left(\frac{t}{\tau}\right)^{\alpha-\beta}u_{l2}(x,t)\right\}, \quad t > \tau, \end{aligned} \tag{3.22}$$

where $u_{l1}(x,t)$ and $u_{l2}(x,t)$ are given by

$$u_{l1}(x,t)=\sum_{n=0}^{\infty}\frac{(-1)^n}{n!}\left[\frac{p_2}{p_1}\left(\frac{t}{\tau}\right)^{\alpha-\beta}\right]^n H_{2,3}^{2,1}\left[\frac{p_1(1+\varepsilon_0)x^2}{4\tau^{1-\alpha}t^{\alpha}}\,\middle|\,\begin{matrix}(0,2);\left(1+(\alpha-\beta)n-\frac{\alpha}{2},\alpha\right)\\(0,1),\left(\frac{1}{2}+n,1\right);(-1,2)\end{matrix}\right],$$
$$u_{l2}(x,t)=\sum_{n=0}^{\infty}\frac{(-1)^n}{n!}\left[\frac{p_2}{p_1}\left(\frac{t}{\tau}\right)^{\alpha-\beta}\right]^n H_{2,3}^{2,1}\left[\frac{p_1(1+\varepsilon_0)x^2}{4\tau^{1-\alpha}t^{\alpha}}\,\middle|\,\begin{matrix}(0,2);\left(1+(\alpha-\beta)(n+1)-\frac{\alpha}{2},\alpha\right)\\(0,1),\left(\frac{1}{2}+n,1\right);(-1,2)\end{matrix}\right]. \quad (3.23)$$

For the very large values of time, $t\to\infty$, the displacement is given by

$$u_{\alpha}(x,t)=U_{-\infty}\exp(-at)\cos(bt)+\frac{\Theta_0}{2}\mathscr{H}(t)$$
$$+\Theta_0\sqrt{\frac{p_1(1+\varepsilon_0)}{4\pi\tau^{1-\alpha}t^{\alpha}}}H_{2,3}^{2,1}\left[\frac{p_1(1+\varepsilon_0)x^2}{4\tau^{1-\alpha}t^{\alpha}}\,\middle|\,\begin{matrix}(0,2);\left(1-\frac{\alpha}{2},\alpha\right)\\(0,1),\left(\frac{1}{2},1\right);(-1,2)\end{matrix}\right],\quad t\to\infty. \quad (3.24)$$

It is evident from the long-time domain solutions that $\theta_{\alpha}(x,t)$ can be extracted from (3.19) and (3.20), and $u_{\alpha}(x,t)$ can be obtained from (3.22) by setting $p_2=0$.

4. Numerical discussions

This part discusses the closed-form formulas of temperature $\theta(x,t)$, hydrostatic stress $\sigma_H(x,t)$, and displacement $u(x,t)$ derived in the preceding section. For this goal, we utilize the series expansion (A.6) for representing the Fox H-function in the above solutions. The Fox H-function of the temperature short-time domain solution (3.8)-(3.9) and the temperature long-time domain solution (3.19)-(3.20) can be represented in terms of the elementary gamma function as

$$H_{1,2}^{2,0}\left[z\,\middle|\,\begin{matrix}(a_1,A_1)\\(0,1),\left(\frac{1}{2}+n,1\right)\end{matrix}\right]=\sum_{\nu=0}^{\infty}\frac{(-z)^{\nu}}{\nu!}\left[\frac{\Gamma\left(\frac{1}{2}+n-\nu\right)}{\Gamma(a_1-A_1\nu)}+z^{\frac{1}{2}+n}\frac{\Gamma\left(-\frac{1}{2}-n-\nu\right)}{\Gamma\left(a_1-A_1\left(\left(\frac{1}{2}+n+\nu\right)\right)\right)}\right]. \quad (4.1)$$

On the other hand, the Fox H-function of the displacement short-time domain solution (3.15) and (3.16), and the displacement long-time domain solution (3.22) and (3.23) can be represented in terms of the elementary gamma function as

$$H_{2,3}^{2,1}\left[z\,\middle|\,\begin{matrix}(0,2);(a_1,A_1)\\(0,1),\left(\frac{1}{2}+n,1\right);(-1,2)\end{matrix}\right]=$$
$$\sum_{\nu=0}^{\infty}\frac{(-z)^{\nu}}{\nu!}\left[\frac{\Gamma\left(\frac{1}{2}+n-\nu\right)}{(1+2\nu)\Gamma(a_1-A_1\nu)}+z^{\frac{1}{2}+n}\frac{\Gamma\left(-\frac{1}{2}-n-\nu\right)}{2(1+n+\nu)\Gamma\left(a_1-A_1\left(\left(\frac{1}{2}+n+\nu\right)\right)\right)}\right]. \quad (4.2)$$

We select the copper material (Cu) with the thermophysical properties at room temperature 300 K for the numerical simulations:

$$\varepsilon_0=0.0168,\quad \delta_0=0.5013,\quad c_1\eta=3.695\times10^{7}\mathrm{m}^{-1},\quad c_1^2\eta=1.536\times10^{11}\mathrm{sec}^{-1}. \quad (4.3)$$

Furthermore, we assign the following values for the dimensionless constants τ, Θ_0 and $U_{-\infty}$:

$$\tau = 0.1, \quad \Theta_0 = 1, \quad U_{-\infty} = 1. \tag{4.4}$$

Unless specified differently, we select the following model parameters for our computations:

$$\alpha = 0.3, \quad \beta = 0.8, \quad p_1 = p_2 = 0.5. \tag{4.5}$$

The series (3.8)-(3.9) and (3.19)-(3.20) with the H-function representation (4.1) are directly implemented to numerically calculate the temperature in the short-time and in the long-time domains, respectively. On the other hand, the series (3.15)-(3.16) and (3.22)-(3.23) with the H-function representation (4.2) are used directly to compute the displacement numerically in the short- and long-time domains, respectively. The summations are carried out over the range of 0 to 50, meaning that all series have been truncated in the fifty-first term for all computations. Convergence was verified by increasing the number of terms up to 80, 100, and 120, with no significant changes in the results. However, for a significantly larger number of terms (beyond 150), numerical divergence is observed due to instability and accumulation of round-off errors. Therefore, the adopted truncation ensures both accuracy and stability of the computed results. Namely, the collocation technique is adopted due to its compatibility with the semi-analytical series solution and its efficiency in handling unbounded domains. Unlike domain-based numerical methods such as the finite element method, which require artificial truncation of the domain, the present approach avoids such approximations and provides accurate results with reduced computational effort. In Figure 2, we compare the temperature solution in the short-time domain, (3.8)-(3.9), with the temperature solution (3.11), which can be derived from (3.8) and (3.9) by setting $p_1 = 0$, at different positions $x = 0$, 0.1, and 0.5. Because the solution (3.8) and (3.9) is a part of a generic solution emulating a crossover thermal conduction phenomenon from a relatively high thermal conductivity κ_β in the short-time domain to a relatively low thermal conductivity κ_α in the long-time domain, it coincides well with the temperature solution (3.11) as $t \to 0$, which agrees with the limit (3.18). In Figure 3, a similar comparison is carried out between the long-time domain temperature solution (3.19)-(3.20) at different positions $x = 0$, 1, and 3, and the temperature solution $\theta_\alpha(x,t)$, in (3.21), which uses the thermal energy balance equation

$$\frac{p_1}{\tau^{1-\alpha}} {}_0^C\mathscr{D}_t^\alpha \left(\theta_\alpha + \varepsilon_0 \frac{\partial u_\alpha}{\partial x}\right) = \frac{\partial^2 \theta_\alpha}{\partial x^2}, \tag{4.6}$$

with a single fractional derivative of order α, and can be derived from (3.19)-(3.20) by putting $p_2 = 0$. The coincidence between the two solutions at the very large values of time is clear and suggests the limit $\lim_{t\to\infty} \theta(x,t) = \theta_\alpha(x,t)$.

In Figure 4, we represent the temporal evolution of both the short-time domain temperature solution (3.8) and (3.9) and the long-time domain temperature solution (3.19) and (3.20) at different positions $x = 0$, 0.1, and 0.3. It is evident from all positions, Figure 4a–c, that the short-time solution (3.8)-(3.9) starts to diverge for $t > 0.9$, and the long-time solution starts to diverge for $t < 1$, in other words, the time interval $(0.9, 1)$ can not exactly predicted using the derived solution and there is always a difference between the two solutions at any point inside this interval. In fact, this time interval is correlated to the auxiliary functions in Figure 1, and to the turning point $\Re\{s\} = 10$, which is in turn

determined based on the selection of the characteristic time τ, i.e., $\tau = 0.1$. In a previous study [44], when the characteristic time is set to $\tau = 1$, the turning point is $\Re\{s\} = 1$, and the discontinuity point is at $t = 15$. It should be emphasized that the apparent discontinuity in the interval $(0.9, 1)$ is not physical. The thermoelastic fields are expected to remain continuous in time. The observed gap arises from the use of separate asymptotic solutions valid in the short-time and long-time domains. In the intermediate region, neither approximation is sufficiently accurate, leading to a loss of numerical reliability. This limitation is inherent to the asymptotic approach rather than the underlying model. More refined techniques, such as numerical inversion of the Laplace transform or hybrid approximation schemes, may be employed in future work to obtain a uniformly valid solution.

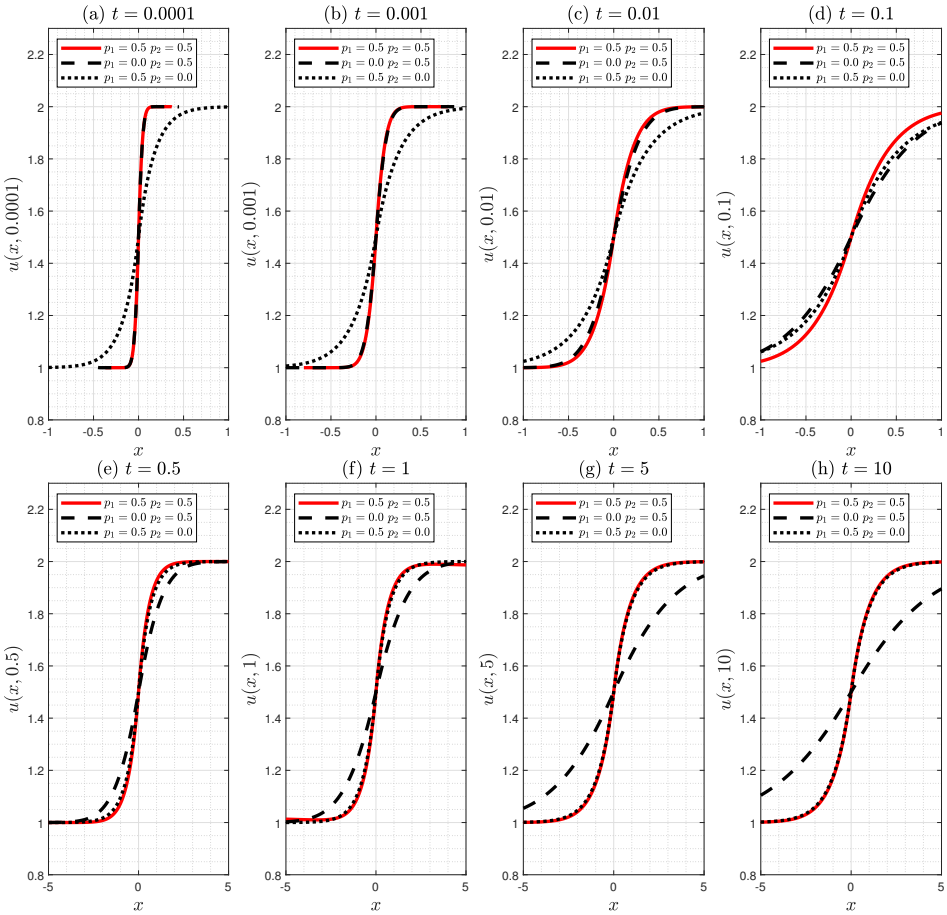

Figure 5. Spatial distribution of the displacement $u(x, t)$ at different values of the dimensionless time t compared with the displacement calculated by fractional thermoelasticity with a single fractional derivative, i.e., Eq (3.17), or Eqs (3.15)–(3.16) with $p_1 = 0$, $p_2 = 0.5$, and Eq (3.24) or Eqs (3.22)–(3.23) with $p_1 = 0.5$, $p_2 = 0$. The selection $a = 0$ and $b = 0$ is considered. The fractional parameters are chosen as $\alpha = 0.3$, $\beta = 0.8$. (a) $t = 0.0001$; (b) $t = 0.001$; (c) $t = 0.01$; (d) $t = 0.1$; (e) $t = 0.5$; (f) $t = 1$; (g) $t = 5$; (h) $t = 10$.

The spatial distribution of displacement at different instants of time are presented in Figure 5. We compare the displacement solutions for short-time domain (3.15) and (3.16), and for long-time domain (3.22) and (3.23), with the displacement solutions of the fractional theory of thermoelasticity with a single fractional derivative of order β, refer to $u_\beta(x, t)$ in (3.17), or a single fractional derivative of order

α refer to $u_\alpha(x,t)$ in (3.24). The red curves in the subplots of Figure 5a–e are drawn using the short-time domain solution (3.15) and (3.16), whereas the red curves in Figure 5f–h are drawn using the long-time domain solution (3.22) and (3.23). The temporal crossover behavior of the red curve from the short-time domain, in which it matches with the dashed curve $u_\beta(x,t)$, to the long-time domain, in which it coincides with the dotted curve $u_\alpha(x,t)$, is evident and emphasizes the main peculiarity of the proposed model. It is noticed that the limit $\lim_{t\to\infty} u(x,t) = u_\alpha(x,t)$ holds true. Furthermore, we consider in Figure 5 the infinite boundary condition with unity ($U_{-\infty} = 1$) where we choose $a = 0$ and $b = 0$, i.e., neglecting the effect of damped wave boundary condition. This choice reduces Eq (3.14) to

$$u(x,t) = \frac{3}{2} + \int_0^x \theta(\xi,t)\mathrm{d}\xi, \quad t \geq 0. \tag{4.7}$$

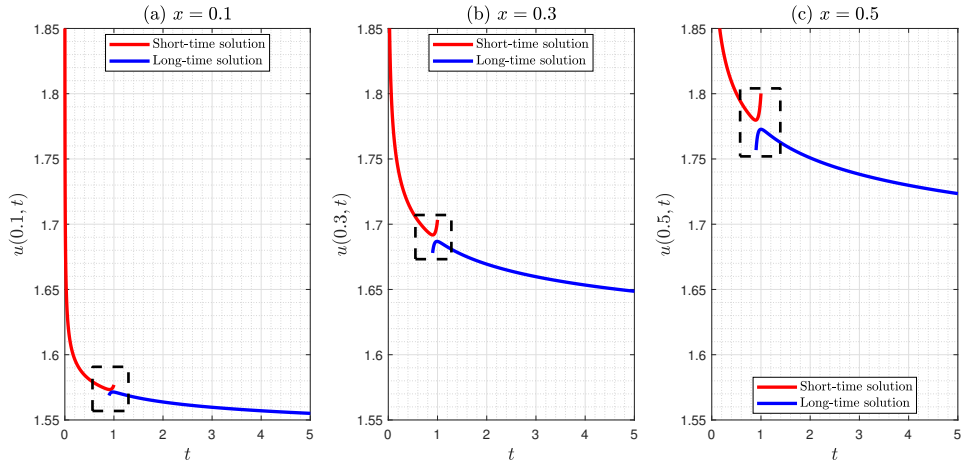

Figure 6. Temporal evolution of the short-time and the long-time displacement solutions (3.15)-(3.16) and (3.22)-(3.23), respectively, at different positions: (a) $x = 0.1$; (b) $x = 0.3$; (c) $x = 0.5$.

Therefore, using the normalization condition (2.44), we have that $u(-\infty,t) = 1$, $u(0,t) = 3/2$, and $u(\infty,t) = 2$, i.e., the displacement curve tends to be step-like shape. This behavior is due to neglecting the mechanical wave, or in other words, the quasistatic assumption. On the other hand, to explore the temporal range in which both displacement solutions in the short-time domain (3.15) and (3.16), and in the long-time domain (3.22) and (3.23), are effective, we study their temporal evolution in Figure 6, at different positions $x = 0.1$, 0.3, and 0.5. as predicted from the temperature solution, refer to Figure 4, Figure 6 shows that the displacement solution for short-time domain may diverge for $t > 0.9$, and the displacement solution for the long-time domain may diverge for $t < 1$, namely, the displacement can be barely drawn on the interval $(0.9, 1)$.

The displacement contours along the spatial domain $(-5, 5)$ and on the temporal domain $(0.001, 50)$ is presented in Figure 7 for different values of the damping factor a and the frequency b. Figure 7 a exhibits the displacement contour on the spatio-temporal domain, as the case in Figure 5, wherein both the damping factor and the frequency are disregarded so that the displacement is always passing from $u(-\infty,t) = 1$ to $u(\infty,t) = 2$, through $u(0,t) = 3/2$. The damping factor is set to $a = 0.1$ in Figure 7 b, and its effect is clear as the time prolongs. Figure 7 c represents the displacement contours when the boundary condition is an undamped cosinusoidal wave, i.e., $a = 0$ and $b = 1$, and Figure 7

d represents the displacement contours when the boundary condition is a damped cosinusoidal wave, i.e., $a = 0.1$ and $b = 1$. The effect of the infinite boundary condition on the elastic medium is due to the absence of finite mechanical wave speed. If the dynamic theory is considered in a future study, obtaining such results will be impossible. The displacement directions are predicted to be changed with the boundary condition (3.13). In Figure 8, we show how the direction of the displacement may be changed in the case of damped and undamped cosinusoidal boundary condition. In Figures 8a,b, in which the oscillation frequency is set to zero, the displacement direction is fixed.

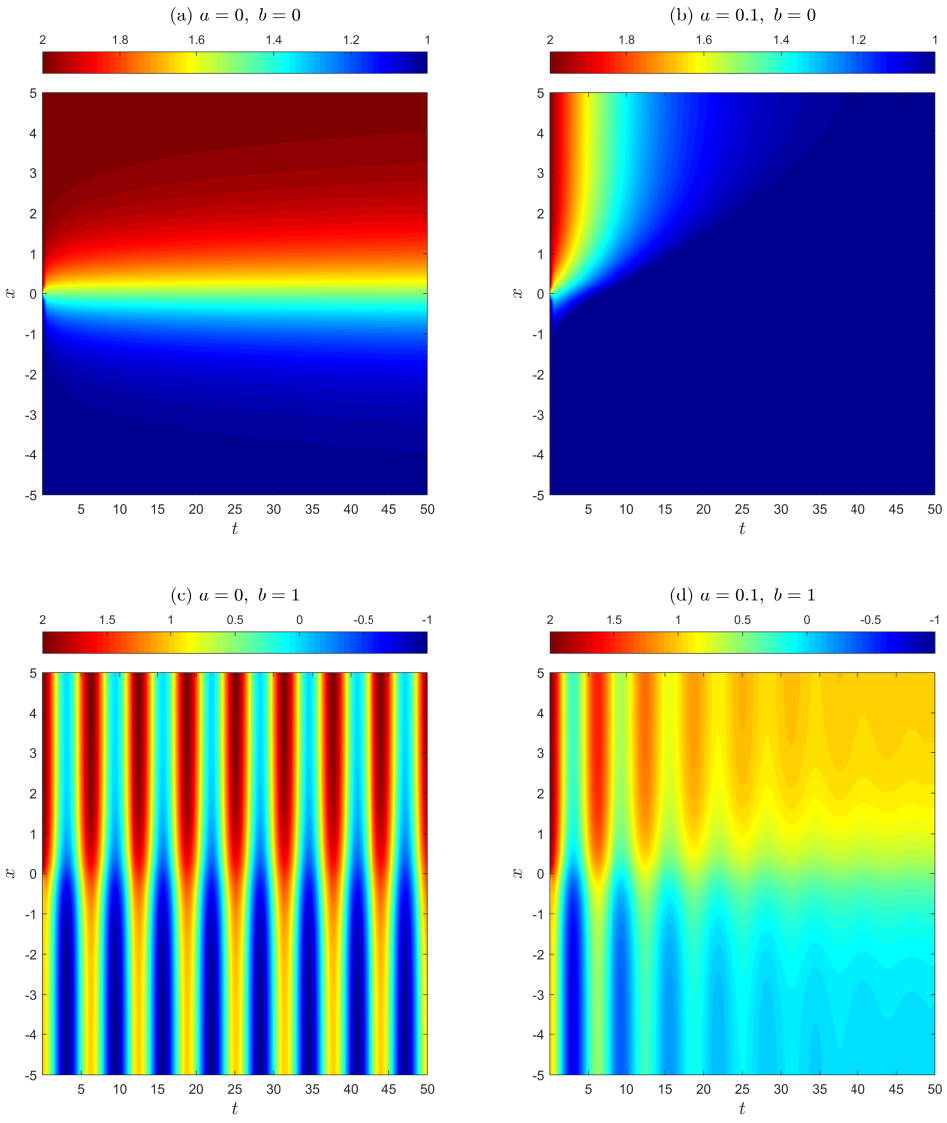

Figure 7. Displacement contours computed from both the short-time and the long-time solutions (3.15)-(3.16) and (3.22)-(3.23), respectively, for different values of the damping coefficient a and the frequency b. (a) $a = 0$ and $b = 0$; (b) $a = 0.1$ and $b = 0$; (c) $a = 0$ and $b = 1$; (d) $a = 0.1$ and $b = 1$.

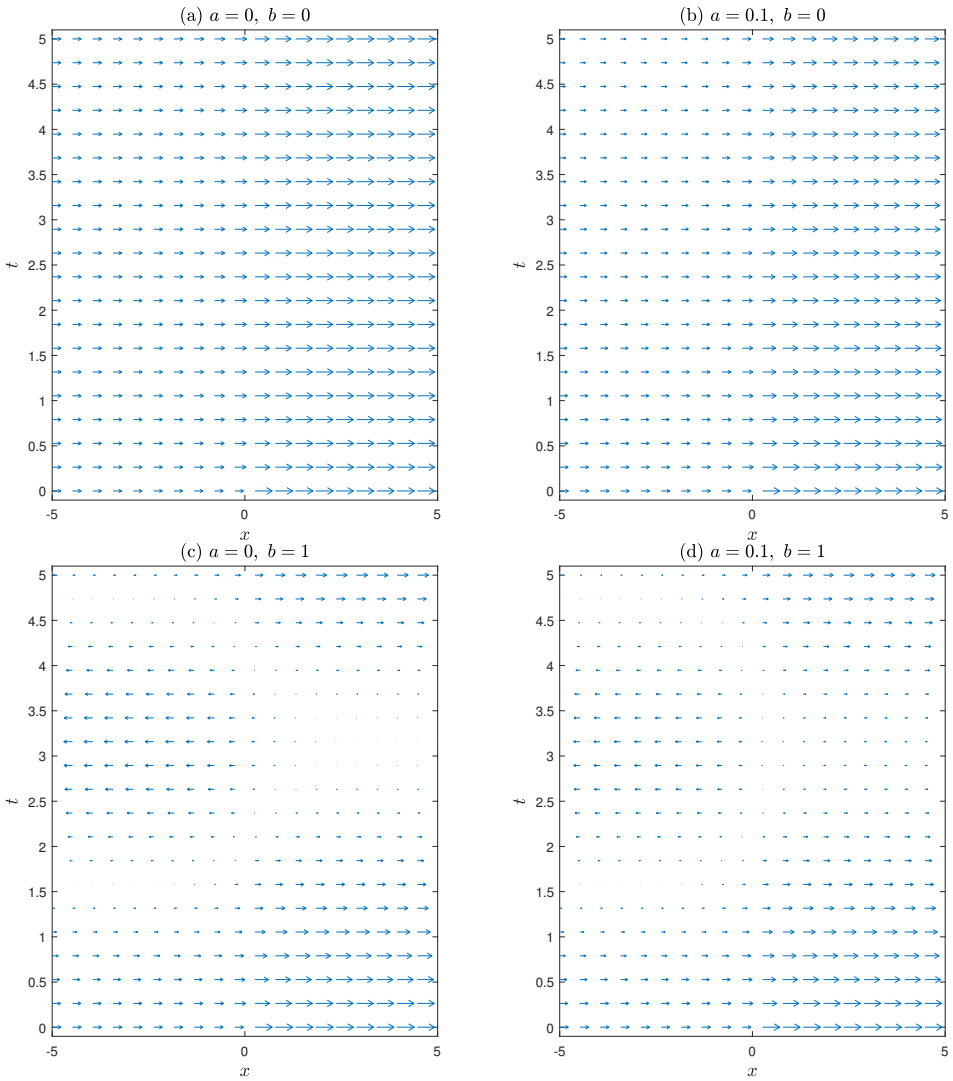

Figure 8. Displacement vectors computed from both the short-time and the long-time solutions (3.15)-(3.16) and (3.22)-(3.23), respectively, for different values of the damping coefficient a and the frequency b. (a) $a = 0$ and $b = 0$; (b) $a = 0.1$ and $b = 0$; (c) $a = 0$ and $b = 1$; (d) $a = 0.1$ and $b = 1$.

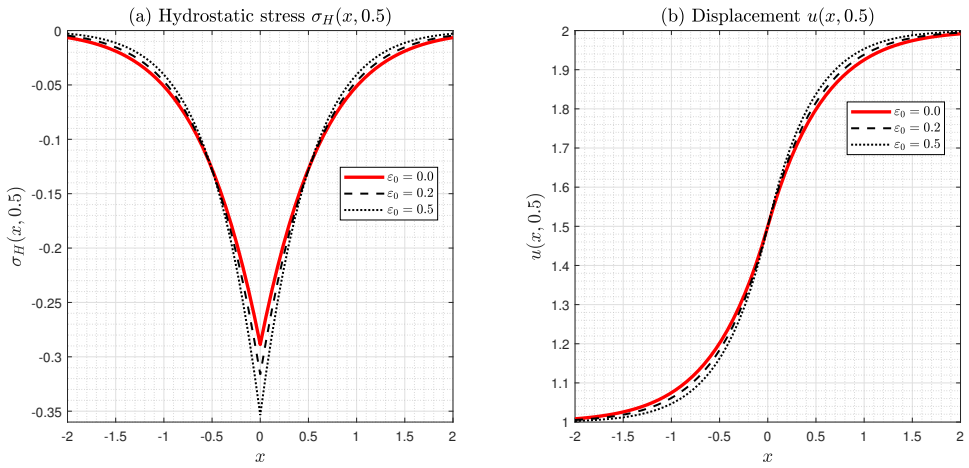

Figure 9. Effect of the thermoelastic coupling ε_0 on the hydrostatic stress (2.38) and the displacement at the dimensionless time $t = 0.5$, and at three different values of ε_0, $\varepsilon_0 = 0$, 0.2, and 0.5: (a) Hydrostatic stress; (b) Displacement.

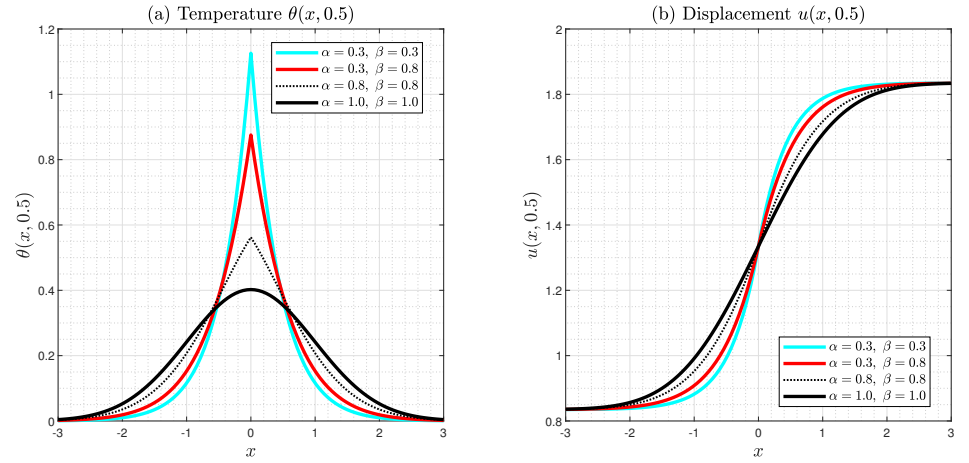

Figure 10. Comparison between the proposed model of decelerating thermal conduction with low thermal conduction $\alpha = 0.3$, $\beta = 0.3$, decelerating thermal conduction $\alpha = 0.3$, $\beta = 0.8$, relatively high thermal conduction $\alpha = 0.8$, $\beta = 0.8$, and the classical model of Fourier thermal conduction $\alpha = 1$, $\beta = 1$: (a) Temperature; (b) Displacement.

The effect of the thermoelastic coupling ε_0 on the hydrostatic stress and the displacement is studied in Figure 9. Three different values for ε_0 are proposed, $\varepsilon_0 = 0$, 0.2, 0.5. The case $\varepsilon_0 = 0$ represents the uncoupled theory in which the mechanical effect on the thermal energy is neglected. The hydrostatic stress $\sigma_H(x, t = 0.5)$ is computed from (2.38) which requires the temperature solution for short-time domain (3.8) and (3.9). As ε_0 increases, the mechanical effect on the thermal wave increases the hydrostatic stress inside the medium and thereby increases the deformation as displacement exhibits in Figure 8 b. it is salient that the discontinuity of the stress disappears due to the quasistatic assumption.

In the limiting case where the fractional orders tend to unity, the proposed model reduces to the classical Fourier heat conduction equation. In Figure 10, we compare four regimes of heat transfer: (a) Low thermal conduction $\alpha = 0.3$, $\beta = 0.3$, (b) decelerating thermal conduction $\alpha = 0.3$, $\beta = 0.8$,

(c) relatively high thermal conduction $\alpha = 0.8$, $\beta = 0.8$, and (d) classical model of Fourier thermal conduction $\alpha = 1$, $\beta = 1$, see recent examples in [55, 56]. The universality of the proposed model stems from its ability to capture more than one regime of thermal conduction. The classical Fourier is clearly the fame bell-shaped of the normal distribution. The numerical results confirm that the fractional solutions converge smoothly to the classical solution, demonstrating the consistency of the formulation.

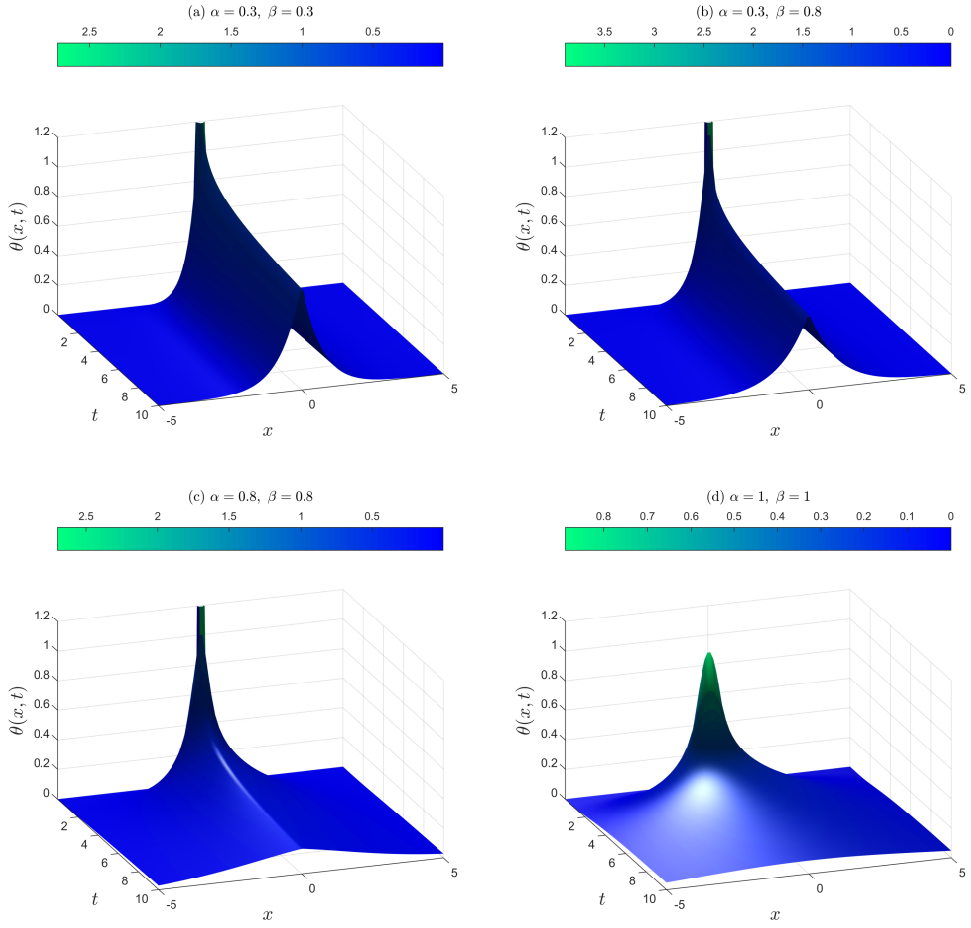

Figure 11. The temporal-spatial evolution of temperature governed by four regimes of thermal conduction: (a) Low thermal conduction $\alpha = 0.3$, $\beta = 0.3$, (b) Decelerating thermal conduction $\alpha = 0.3$, $\beta = 0.8$, (c) relatively high thermal conduction $\alpha = 0.8$, $\beta = 0.8$, and (d) Classical model of Fourier thermal conduction $\alpha = 1$, $\beta = 1$.

For further depiction of the nature of the temperature governed by the proposed crossover model, in Figure 11, the temperature evolution over the spatial domain $(-3, 3)$ and the temporal domain $(0, 10)$ is represented for four regimes of heat transfer that can be modeled using the proposed model: (a) Low thermal conduction $\alpha = 0.3$, $\beta = 0.3$, (b) decelerating thermal conduction $\alpha = 0.3$, $\beta = 0.8$, (c) relatively high thermal conduction $\alpha = 0.8$, $\beta = 0.8$, and (d) classical model of Fourier thermal conduction $\alpha = 1$, $\beta = 1$.

5. Summary

In this work, we have suggested an unfamiliar generalized Fourier constitutive law of distributed-order Riemann-Liouville integral. Using a specific choice of the weight function, we obtain a bi-fractional Fourier constitutive law including two Riemann-Liouville integrals with distinct orders. The considered constitutive law is phenomenologically and numerically shown to simulate heat conduction situations with a transitional behavior from a relatively high thermal conductivity κ_β in the short-time domain to a relatively low thermal conductivity κ_α in the long-time domain, namely, a decelerating thermal conduction. Moreover, we have studied the effect of this transitional behavior of thermal conduction on the deformation of unbounded perfectly elastic domain by deriving exact solutions for the displacement. For making the problem more tractable, we consider the quasistatic theory of thermoelasticity in which the inertial term $\varrho\partial^2 u/\partial t^2$ is absent.

We have considered two groups of initial conditions. One of them imposes zero initial-state on the stress, and the other imposes zero initial-state on the cubical dilation. We found that the zero initial-state on the cubical dilation contradicts the quasistatic assumption, for this reason, the second group was excluded from the analysis. Although the initial conditions suggested in the first group were sufficient for establishing the temperature solution, an extra boundary condition at $x \to -\infty$ is found to be necessary for the displacement solution to ensure generality.

The idea of conditional solutions, as introduced in [51], has been generalized in this study to obtain two different solutions; one is applicable for small values of time ($t \leq 0.9$), and the second is applicable for intermediate and large values of time ($t \geq 1$). Although the adopted approach enables us to address a wide time range, there is an interval $(0.9, 1)$ contains discontinuous point between the two solutions, and the solution can be barely computed inside this interval after maneuvers to search for and avoid the discontinuity point.

The key finding of the present study is depicted in Figure 5, which illustrates that the displacement of the medium reflects the same temporal crossover behavior, shifting from the displacement caused by the high thermal conduction during the very small time values to the displacement caused by the low thermal conduction during the very large time values, indicating a trend of decelerating deformation of the elastic medium. The suggested model of thermoelasticity with decelerating thermal conduction is currently in its initial phases and requires further application and testing. In future plans, we will apply this model to different geometries, and composite materials. Moreover, the inertial term $\varrho\partial^2 u/\partial t^2$ should be considered in the presence of such a decelerating crossover. The sensitivity analysis indicates that the thermoelastic coupling parameter ε_0 has a pronounced effect on both the qualitative and quantitative behavior of the solution, whereas the remaining parameters, δ_0 and Θ_0, mainly influence the amplitude of the temperature and displacement fields without modifying the overall trends.

Appendix

A. Special functions

Here, we summarize the special functions used throughout the paper. We begin with the Mittag-Leffler function with three parameters $E^{\gamma}_{\alpha,\beta}(\cdot)$, known also as the Prabhakar generalization of Mittag-

Leffler function (PML), and defined as [57, 58]

$$E_{\alpha,\beta}^{\gamma}(z) = \sum_{n=0}^{\infty} \frac{(\gamma)_n}{\Gamma(\alpha n + \beta)} \frac{z^n}{n!}, \quad z \in \mathbb{C}, \quad \Re\{\alpha\}, \ \Re\{\beta\}, \Re\{\gamma\} > 0, \tag{A.1}$$

where $(\gamma)_n$is the ascending Pochhammer symbol defined by $(\gamma)_0 = 1$, $(\gamma)_n = \gamma(\gamma+1)\cdots(\gamma+n-1) = \frac{\Gamma(\gamma+n)}{\Gamma(\gamma)}$. The Laplace transform of the generalized Mittag-Leffler function is provided by

$$\mathscr{L}^{-1}\left\{\frac{s^{\alpha\gamma-\beta}}{(s^{\alpha}+\lambda)^{\gamma}}\right\} = t^{\beta-1}E_{\alpha,\beta}^{\gamma}(-\lambda t^{\alpha}), \quad \Re\{\alpha\}, \ \Re\{\beta\}, \Re\{\gamma\} > 0. \tag{A.2}$$

The generalized Mittag-Leffler function is defined through the following relation

$$E_{\alpha,\beta}^{\gamma}(-z) = \frac{1}{\Gamma(\gamma)} H_{1,2}^{1,1}\left[z \,\middle|\, \begin{matrix}(1-\gamma,1)\\(0,1),(1-\beta,\alpha)\end{matrix}\right], \tag{A.3}$$

where $H_{p,q}^{m,n}[\cdot]$ is the Fox H-function defined in terms of the Mellin-Barnes integral [59] as

$$H_{p,q}^{m,n}\left[x \,\middle|\, \begin{matrix}(a_1,A_1),\cdots,(a_p,A_p)\\(b_1,B_1),\cdots,(b_q,B_q)\end{matrix}\right] = \frac{1}{2\pi\imath}\int_{\Omega}\Theta(s)\,x^{s}\,ds, \tag{A.4}$$

$m,\ n,\ p$, and q are integers satisfying $0 \le n \le p$, $1 \le m \le q$, $a_i,\ b_j \in \mathbb{C}$, $A_i,\ B_j \in \mathbb{R}_+$, $i = 1,\cdots,p$, $j = 1,\cdots,q$, and the function $\Theta(s)$ is given by

$$\Theta(s) = \frac{\prod_{j=1}^{m}\Gamma(b_j - B_j s)\prod_{j=1}^{n}\Gamma(1-a_j+A_j s)}{\prod_{j=m+1}^{q}\Gamma(1-b_j+B_j s)\prod_{j=n+1}^{p}\Gamma(a_j - A_j s)}, \tag{A.5}$$

where $\Gamma(\cdot)$ is the Gamma function. The contour Ω on the right-hand side of Eq (A.4) separates the poles of $\Gamma(b_j + B_j s)$, $j = 1,\cdots,m$ from the poles of $\Gamma(1-a_i-A_i s)$, $i = 1,\cdots,n$.

If the poles of $\prod_{j=1}^{m}\Gamma(b_j - B_j s)$ are simple, the following series expansion holds true

$$\begin{aligned} H_{p,q}^{m,n}\left[x \,\middle|\, \begin{matrix}(a_p,A_p)\\(b_q,B_q)\end{matrix}\right] &= \sum_{h=1}^{m}\sum_{\nu=0}^{\infty}\frac{(-1)^{\nu}x^{\frac{b_h+\nu}{B_h}}}{\nu!B_h}\times \\ &\times\frac{\prod_{j=1,j\neq h}^{m}\Gamma\left(b_j - B_j\frac{b_h+\nu}{B_h}\right)\prod_{j=1}^{n}\Gamma\left(1-a_j+A_j\frac{b_h+\nu}{B_h}\right)}{\prod_{j=m+1}^{q}\Gamma\left(1-b_j+B_j\frac{b_h+\nu}{B_h}\right)\prod_{j=n+1}^{p}\Gamma\left(a_j - A_j\frac{b_h+\nu}{B_h}\right)} \end{aligned} \tag{A.6}$$

The inverse Fourier transform of the H -function $H_{1,2}^{1,1}\left[a|\omega|^{\delta}\right]$ is given by (derived in [51])

$$\begin{aligned} &\mathscr{F}^{-1}\left\{|\omega|^{\lambda}H_{1,2}^{1,1}\left[a|\omega|^{\delta}\,\middle|\,\begin{matrix}(-n,1)\\(0,1);(\beta,\gamma)\end{matrix}\right]\right\}(x) \\ &\qquad = \frac{1}{\sqrt{4\pi}a^{\frac{\lambda+1}{\delta}}}H_{2,3}^{2,1}\left[\frac{|x|^{\delta}}{2^{\delta}a}\,\middle|\,\begin{matrix}\left(1-\frac{\lambda+1}{\delta},1\right);\left(1-\beta-\frac{\lambda+1}{\delta}\gamma,\gamma\right)\\\left(0,\frac{\delta}{2}\right),\left(1+n-\frac{\lambda+1}{\delta},1\right);\left(\frac{1}{2},\frac{\delta}{2}\right)\end{matrix}\right], \end{aligned} \tag{A.7}$$

where ω is the Fourier parameter, $a,\ \gamma,\ \delta \in \mathbb{R}_+$, $\beta, n \in \mathbb{C}$, and $\lambda \in \mathbb{R}_+ \cup \{0\}$.

The following reduction property is employed throughout the paper, refer to relation [(1.56), p. 11 in [59]]

$$H_{p,q}^{m,n}\left[x\left|\begin{array}{c}(a_1,A_1),\cdots,(a_p,A_p)\\(b_1,B_1),\cdots,\left(b_{q-1},B_{q-1}\right),(a_1,A_1)\end{array}\right.\right]$$
$$=H_{p-1,q-1}^{m,n-1}\left[x\left|\begin{array}{c}(a_2,A_2),\cdots,(a_p,A_p)\\(b_1,B_1),\cdots,\left(b_{q-1},B_{q-1}\right)\end{array}\right.\right], \tag{A.8}$$

provided that $n \geq 1$ and $q > m$.

We introduce the Euler transform of the Fox H-function, [see p. 59 in [59]], as follows

$$\int_0^t x^{\rho-1}(t-x)^{\sigma-1}H_{p,q}^{m,n}\left[bx^k\left|\begin{array}{c}\left(a_p,A_p\right)\\\left(b_q,B_q\right)\end{array}\right.\right]\mathrm{d}x$$
$$=t^{\rho+\sigma-1}\Gamma(\sigma)\,H_{p+1,q+1}^{m,n+1}\left[bt^k\left|\begin{array}{c}(1-\rho,k),\left(a_p,A_p\right)\\\left(b_q,B_q\right),(1-\rho-\sigma,k)\end{array}\right.\right], \tag{A.9}$$

where $\rho, \sigma, b \in \mathbb{C}$, and $k > 0$.

Author contributions

Emad Awad: Writing – review & editing, Writing – original draft, Software, Formal analysis, Methodology, Conceptualization; Amr R. El-Dhaba: Writing– review & editing, Writing – original draft, Software, Formal analysis, Methodology, Conceptualization. All authors have read and agreed to the published version of the manuscript.

Use of Generative-AI tools declaration

The authors declare they have not used Artificial Intelligence (AI) tools in the creation of this article.

Data availability statement

The data that support the findings of this study are available from the corresponding author upon reasonable request.

Funding

This work was supported by the Deanship of Scientific Research, Vice Presidency for Graduate Studies and Scientific Research, King Faisal University, Saudi Arabia (Grant No–KFU261901).

Conflicts of interest

The authors declare no conflict of interest.

References

1. T. Q. Qiu, C. L. Tien, Heat transfer mechanisms during short-pulse laser heating of metals, *ASME J. Heat Transfer*, **115** (1993), 835–841.
2. Z. M. Zhang, *Nano/microscale heat transfer*, New York: McGraw- Hill, 2007.
3. E. Awad, W. Dai, S. Sobolev, Thermal oscillations and resonance in electron–phonon interaction process, *Z. Angew. Math. Phys.*, **75** (2024), 143. https://doi.org/10.1007/s00033-024-02277-w
4. R. Berman, D. K. C. Macdonald, The thermal and electrical conductivity of sodium at low temperatures, *Proc R Soc (London) A*, **209** (1951), 368–375.
5. J. Hulm, Anomalous thermal conductivity of pure metals at low temperatures, *Proceedings of the Physical Society. Section A*, **65** (1952), 227.
6. G. Busch, M. Schneider, Heat conduction in semiconductors, *Physica*, **20** (1954), 1084–1086.
7. P. Price, Cxxxv. ambipolar thermodiffusion of electrons and holes in semiconductors, *London Edinburgh Philos. Mag. J. Sci.*, **46** (1955), 1252–1260.
8. S. Lepri, R. Livi, A. Politi, On the anomalous thermal conductivity of one-dimensional lattices, *Eur. Lett.*, **43** (1998), 271.
9. B. Li, J. Wang, Anomalous heat conduction and anomalous diffusion in one-dimensional systems, *Phys. Rev. Lett.*, **91** (2003), 044301.
10. V. Lee, C.-H. Wu, Z.-X. Lou, W.-L. Lee, C.-W. Chang, Divergent and ultrahigh thermal conductivity in millimeter-long nanotubes, *Phys. Rev. Lett.*, **118** (2017), 135901.
11. J. S. Kang, M. Li, H. Wu, H. Nguyen, Y. Hu, Experimental observation of high thermal conductivity in boron arsenide, *Science*, **361** (2018), 575–578.
12. W. Lin, J. He, X. Su, X. Zhang, Y. Xia, T. P. Bailey, et al., Ultralow thermal conductivity, multiband electronic structure and high thermoelectric figure of merit in tlcuse, *Adv. Mater.*, **33** (2021), 2104908.
13. S. Guo, S. Chen, A. Nkansah, A. Zehri, M. Murugesan, Y. Zhang, et al., Toward ultrahigh thermal conductivity graphene films, *2D Mater.*, **10** (2022), 014002.
14. D. Li, Y. Wu, P. Kim, L. Shi, P. Yang, A. Majumdar, Thermal conductivity of individual silicon nanowires, *Appl. Phys. Lett.*, **83** (2003), 2934–2936.
15. R. Metzler, J. Klafter, The random walk's guide to anomalous diffusion: A fractional dynamics approach, *Phys. Rep.*, **339** (2000), 1–77.
16. J. Klafter, S. Lim, R. Metzler, *Fractional dynamics: recent advances*, World Scientific, 2012.
17. W. Schneider, W. Wyss, Fractional diffusion and wave equations, *J. Math. Phys.*, **30** (1989), 134–144.
18. A. Chechkin, R. Gorenflo, I. Sokolov, Retarding subdiffusion and accelerating superdiffusion governed by distributed-order fractional diffusion equations, *Phys. Rev. E*, **66** (2002), 046129.
19. I. Sokolov, A. Chechkin, J. Klafter, Distributed-order fractional kinetics, *Acta Phys. Pol. B*, **35** (2004), 1323.

20. E. Awad, T. Sandev, R. Metzler, A. Chechkin, Closed-form multi-dimensional solutions and asymptotic behaviors for subdiffusive processes with crossovers: I. retarding case, *Chaos, Solitons Fractals*, **152C** (2021), 111357.

21. E. Awad, R. Metzler, Closed-form multi-dimensional solutions and asymptotic behaviours for subdiffusive processes with crossovers: Ii. accelerating case, *J. Phys.A: Math. Gen.*, **55** (2022), 205003.

22. F. Mainardi, A. Mura, R. Gorenflo, M. Stojanović, The two forms of fractional relaxation of distributed order, *J. Vib. Control*, **13** (2007), 1249–1268.

23. F. Mainardi, G. Pagnini, The role of the fox–wright functions in fractional sub-diffusion of distributed order, *J. Comput. Appl. Math.*, **207** (2007), 245–257.

24. F. Mainardi, A. Mura, G. Pagnini, R. Gorenflo, Time-fractional diffusion of distributed order, *J. Vib. Control*, **14** (2008), 1267–1290.

25. E. Bazhlekova, I. Bazhlekov, Transition from diffusion to wave propagation in fractional jeffreys-type heat conduction equation, *Fractal Fractional*, **4** (2020), 32.

26. C.-c. Ji, W. Dai, Z.-z. Sun, Numerical method for solving the time-fractional dual-phase-lagging heat conduction equation with the temperature-jump boundary condition, *J. Sci. Comput.*, **75** (2018), 1307–1336, https://doi.org/10.1007/s10915-017-0588-3

27. C.-c. Ji, W. Dai, Z.-z. Sun, Numerical schemes for solving the time-fractional dual-phase-lagging heat conduction model in a double-layered nanoscale thin film, *J. Sci. Comput.*, **81** (2019), 1767–1800. https://doi.org/10.1007/s10915-019-01062-6

28. C.-c. Ji, W. Dai, Sub-diffusion two-temperature model and accurate numerical scheme for heat conduction induced by ultrashort-pulsed laser heating, *Fractal Fractional*, **7** (2023), 319.

29. A. Compte, R. Metzler, The generalized cattaneo equation for the description of anomalous transport processes, *J. Phys. A: Math. Gen.*, **30** (1997), 7277.

30. E. Awad, On the time-fractional cattaneo equation of distributed order, *Phys. A: Stat. Mech. Appl.*, **518** (2019), 210–233.

31. E. Awad, A. A. El-Bary, W. Dai, Linear damped oscillations underlying the fractional jeffreys equation, *Fractal Fract*, **9** (2025), 556. https://doi.org/10.3390/fractalfract9090556

32. M. A. Biot, Thermoelasticity and irreversible thermodynamics, *J. Appl Phys* , **27** (1956), 240–253.

33. J. Ignaczak, M. Ostoja-Starzewski, *Thermoelasticity with Finite Wave Speeds*, New York: Oxford University Press, 2010.

34. M. Abou-Dina, A. El Dhaba, A. Ghaleb, E. Rawy, A model of nonlinear thermo-electroelasticity in extended thermodynamics, *Int. J. Eng. Sci.*, **119** (2017), 29–39.

35. W. Mahmoud, M. S. Abou-Dina, A. R. El Dhaba, A. F. Ghaleb, E. K. Rawy, *A One-Dimensional Problem of Nonlinear Thermo-Electroelasticity with Thermal Relaxation*, Cham: Springer International Publishing, 2018, 505–516.

36. D. Y. Tzou, *Macro-to microscale heat transfer: The lagging behavior*, 2 Eds., John Wiley & Sons, 2014.

37. Y. Z. Povstenko, Fractional heat conduction equation and associated thermal stress, *J. Therm. Stresses*, **28** (2005), 83–102.
38. H. H. Sherief, A. M. A. El-Sayed, A. M. Abd El-Latief, Fractional order theory of thermoelasticity, *Int. J. Solids Struct.*, **47** (2010), 269–275.
39. H. M. Youssef, Theory of fractional order generalized thermoelasticity, *J. Heat Transfer*, **132** (2010), 1–7.
40. M. A. Ezzat, A. S. El Karamany, Theory of fractional order in electro-thermoelasticity, *Eur. J. Mech., A/Solids*, **30** (2011), 491–500.
41. Y. Povstenko, Fractional cattaneo-type equations and generalized thermoelasticity, *J. Thermal Stresses*, **34** (2011), 97–114.
42. E. Awad, On the generalized thermal lagging behavior: Refined aspects, *J. Thermal Stresses*, **35** (2012), 293–325.
43. Y. Z. Povstenko, *Fractional thermoelasticity*, 2 Eds., Cham: Springer, 2024.
44. E. Awad, N. Samir, A closed-form solution for thermally induced affine deformation in unbounded domains with a temporally accelerated anomalous thermal conductivity, *J. Phys. A: Math. Theor.*, **57** (2024), 455202.
45. E. Awad, A. A. El-Bary, H. M. Youssef, Anomalous thermal stresses induced in an infinitely long circular cylinder with accelerated thermal conductivity, *Int. Commun. Heat Mass Transfer*, **167** (2025), 109297.
46. E. Awad, A. A. El-Bary, N. Samir, H. M. Youssef, Numerical and exact solutions to the deformations of unbounded domains induced by time-accelerated thermal conduction and electromagnetic induction, *Z. Angew. Math. Mech.*, **105** (2025), e70161. https://doi.org/10.1002/zamm.70161
47. A. Youssef, N. Amein, N. Abdelrahman, M. Abou-Dina, A. Ghaleb, Nonlinear rayleigh wave propagation in a layered half-space in dual-phase-lag, *Sci. Rep.*, **13** (2023), 2187.
48. H. Sherief, A. M. Abd El-Latief, Effect of variable thermal conductivity on a half-space under the fractional order theory of thermoelasticity, *Int. J. Mech. Sci.*, **74** (2013), 185–189.
49. A. A. Kilbas, H. M. Srivastava, J. J. Trujillo, *Theory and Applications of Fractional Differential Equations*, Amsterdam: Elsevier, 2006.
50. D. E. Carlson, Linear Thermoelasticity, In: *Linear Theories of Elasticity and Thermoelasticity*, Berlin, Heidelberg: Springer, 1973. http://doi.org/10.1007/978-3-662-39776-3_2
51. E. Awad, R. Metzler, Crossover dynamics from superdiffusion to subdiffusion: Models and solutions, *Fractional Calculus Appl. Anal.*, **23** (2020), 55–102. https://doi.org/10.1515/fca-2020-0003
52. R. L. Schilling, R. Song, Z. Vondracek, *Bernstein functions: Theory and applications*, Berlin/Boston: De Gruyter, 2012.
53. R. Gorenflo, Y. Luchko, M. Stojanović, Fundamental solution of a distributed order time-fractional diffusion-wave equation as probability density, *Fractional Calculus Appl. Anal.*, **16** (2013), 297–316.

54. T. Sandev, A. V. Chechkin, N. Korabel, H. Kantz, I. M. Sokolov, R. Metzler, Distributed-order diffusion equations and multifractality: Models and solutions, *Phys. Rev. E*, **92** (2015), 042117.

55. E. Awad, A. R. El-Dhaba, The role of fractional calculus in modeling vibrations of a timoshenko beam influenced by low and high thermal conduction, *Eur. J. Mech.-A/Solids*, **118** (2026), 106100.

56. E. Awad, Asymptotic analysis for cauchy stresses in a semi-infinite space with anomalous thermal conduction, *Fractional Calculus Appl. Anal.*, 2026. https://doi.org/10.1007/s13540-026-00507-8

57. R. Garra, R. Garrappa, The prabhakar or three parameter mittag–leffler function: Theory and application, *Commun. Nonlinear Sci. Numer. Simul.*, **56** (2018), 314–329.

58. E. Bazhlekova, Completely monotone multinomial mittag-leffler type functions and diffusion equations with multiple time-derivatives, *Fractional Calculus Appl. Anal.*, **24** (2021), 88–111.

59. A. M. Mathai, R. K. Saxena, H. J. Haubold, *The H-function: Theory and applications*, Berlin: Springer, 2010.